Finite Element Model of Thermoelastic Damping in MEMS

by

John P. Gorman

B.S. Physics
University of Vermont, 1995

SUBMITTED TO THE DEPARTMENT OF MATERIALS SCIENCE AND ENGINEERING IN PARTIAL FULFILLMENT OF THE REQUIREMENTS FOR THE DEGREE OF

MASTER OF SCIENCE IN MATERIALS SCIENCE AND ENGINEERING
AT THE
MASSACHUSETTS INSTITUTE OF TECHNOLOGY

JUNE 2002

Signature of Author_____
Department of Materials Science and Engineering

Certified by _____
Amy E. Duwel, Ph.D.
Charles Stark Draper Laboratory
Thesis Supervisor

Certified by _____
Eugene A. Fitzgerald
Professor of Materials Science and Engineering
Thesis Advisor

Accepted by _____
Harry L. Tuller
Professor of Ceramics and Electronics Materials
Chair, Departmental Committee on Graduate Students

[THIS PAGE INTENTIONALLY LEFT BLANK]

Finite Element Analysis of Thermoelastic Damping in MEMS

by

John P. Gorman

Submitted to the Department of Materials Science and Engineering on
May 10, 2002, in partial fulfillment of the requirements for the
Degree of Master of Science in Materials Science and Engineering

Abstract

Damping in MEMS resonators was studied experimentally and numerically. Quality factor measurements were performed on Draper gyroscopes made from boron doped silicon wafers with varying amount of germanium (0%, 2%, 23%, 30%). The quality factors of gyroscopes with germanium were measured to be lower than those without germanium, due to increased anelastic damping. Specifically, the decreased thermal conductivity in the devices with germanium causes those devices to experience thermoelastic damping of a greater magnitude than the germanium-free devices. The amount of damping exhibited is found to be well explained by existing analytical expressions for thermoelastic dissipation in a beam model. The governing equations of thermoelasticity dictate that the amount of damping that a resonator undergoes is a function of both material properties as well as device geometry. Damping will become greatest at operating cycle times that are of the same scale as the thermal relaxation times of the device material. Due to the fact that analytical expressions exist for only a few simple geometries, a finite element model was developed to evaluate thermoelastic damping in more complicated geometries. The finite element model is demonstrated to be in good qualitative agreement with the analytical expressions, and is used to analyze the impact of design modifications such as the addition of fillets and anchors to a simple beam model. It is shown that depending on the size scale of the resonator (which dictates the amount of internal damping), these geometric modifications may either hinder or improve resonator damping characteristics.

Technical Supervisor: Amy E. Duwel, Ph.D.
Title: Senior member of the technical staff

Thesis Advisor: Professor Eugene A. Fitzgerald
Title: Professor of Materials Science and Engineering

[THIS PAGE INTENTIONALLY LEFT BLANK]

ACKNOWLEDGMENT
May 10, 2002

Thanks go to all the people at Draper who have helped me and made this work possible: Connie Cardoso, Mauro Passanisi, Marcie Weinstein, Bill Sawyer, Bill Kelleher, Jeff Borenstein, and Neil Barbour. Thanks also to Professor Fitzgerald's group at MIT who supplied us with test material, in particular Matt Currie.

I appreciate the assistance of other students- especially Clark Allred, Kevin King and Ken Avery. They made me explain what I was working on, and in so doing I was able to understand the material better myself.

Thank you Amy Duwel for spending many hours teaching me the principles of gyroscope operation, for providing excellent mentorship, and for always being available for questions. Thank you Professor Fitzgerald for teaching me the properties of electronic materials and sparking my interest in device processing.

And thanks most of all to Andi and Harley for the constant love and support they gave me to make this all happen. I feel truly lucky to have had this opportunity.

This thesis was prepared at The Charles Stark Draper Laboratory, Inc., under IR&D project number 18526.

Publication of this thesis does not constitute approval by Draper or the sponsoring agency of the findings or conclusions contained herein. It is published for the exchange and stimulation of ideas.

John P. Gorman

[THIS PAGE INTENTIONALLY LEFT BLANK]

Contents

List of Figures

Page

List of Tables

Chapter 1

Introduction

Microelectromechanical systems (MEMS) have been developed to scale down and integrate technologies that ultimately have lower power requirements, smaller physical size (and weight), and lower cost than their macroscopic counterparts. Although many of the devices are constructed using techniques borrowed from integrated circuit manufacturing, MEMS depart from static structural design through the inclusion of flexible elements- sensors and actuators whose motions are governed by the electrical and mechanical properties of the materials used in their construction. Any deviation from the predictable physical behavior of these moving pieces may be attributed to some change in their environment, and hence is the basis of various sensing techniques.

Gyroscopes produced at Draper Laboratory sense angular velocity when micromachined vibrating masses are deflected out of their plane of motion by a Coriolis force. The amplitude of the out of plane motion is sensed capacitively and is proportional to the angular rate of rotation. To maintain low energy loss as well as good sensitivity, the damping of the oscillators must be minimized. Operating the gyroscopes under vacuum conditions greatly reduces energy loss, but further improvements in performance must be based on an understanding of the internal damping mechanisms. To this end, damping measurements were performed on a set of gyroscopes made from different silicon-based compositions. These measurements clearly established that material damping was a factor and deserved further study.

Based upon a literature review of damping mechanisms in quartz oscillators, thermoelastic damping was identified as a leading contributor to energy loss in Draper's gyroscopes. The amount of thermoelastic damping present during device operation depends heavily upon the thermal properties of the doped silicon, which varies markedly among the materials. Specifically, the thermal conductivity had the greatest variation- differing by almost a factor of fifteen for two of the materials in the study. Using analytical expressions developed in papers by Zener and Roukes [1,2,3] for thermoelastic damping in vibrating beams, it is found that thermoelastic damping offers a good

explanation of the differences in measured quality factors of the devices under study. Due to the fact that analytical expressions exist for only a few simple geometries, approximations must be made in the application of the equations to the gyroscope under study. This restraint on the use of the damping equations presented the motivation to develop a general method to calculate thermoelastic damping for an expanded set of geometries.

Finite element analysis was used to develop a method to evaluate the amount of damping in more complex geometries. The partial differential equations that govern the coupling of the strain field and the thermal field were identified along with the appropriate boundary conditions. These were entered into FEMLAB to be solved over various three dimensional geometries. The results of these simulations were compared to the analytical expressions and are found to be in good agreement in regions of maximum damping. Although finite element analysis has been used in the past to study the coupling of the elastic and thermal fields that exist in a material [4,5], typical interest has been limited to static and quasi-static conditions. This work differs from previous research in that the finite element method was employed to solve for complex eigenvalues of oscillatory systems undergoing thermoelastic damping. The ratio of the real and imaginary parts of the eigenvalues is related to the amount of energy lost per radian of oscillation, and hence determines the quality factor of the resonator. This model may be used to quickly evaluate the contribution of thermoelastic damping to new MEMS designs that are still in the developmental stage, and serves as a tool to screen out flawed designs before they go to processing. This work may be extended to other damping mechanisms (that are expressible in terms of partial differential equations) to develop a full suite of models to predict anelastic damping in MEMS.

The goal of this thesis is to present the results of an effort to improve the performance of Draper's gyroscope through a study of the impact of materials selection and beam geometry upon the mechanical quality factor of the oscillator. The thesis comprises two sections; Section 1 contains four chapters that outline the experimental portion of this thesis. Chapter 2 provides the reader with an explanation of the mechanical quality factor (Q) of a resonant structure, Chapter 3 describes Draper's gyroscope (principles of operation and construction), Chapter 4 details the experimental

setup and results of Q measurements, and Chapter 5 uses equations from thermoelastic theory to explain the difference in measured Q values between different materials used to construct the gyroscopes.

Section 2 contains 4 chapters, which describe the physics of the damping mechanism and the development of the finite element model used to predict the amount of damping in a structure due to thermoelastic damping. Chapter 6 is concerned with anelastic materials and resulting damping behavior, Chapter 7 provides detail on thermoelastic damping, Chapter 8 documents the construction of a finite element model with anelastic behavior, and Chapter 9 discusses the features and results of this simulation.

The thesis ends with a conclusion of the information presented, and also contains some thoughts on extending the present body of work.

Section One

This section is designed to provide the reader with a general understanding of the quality factor measurements of Draper Laboratory's gyroscopes, as well as offer a cursory explanation of the difference in measured quality factors between gyroscopes made of different materials. The experimental data clearly identified thermoelastic damping as an important mechanism, motivating the subsequent numerical studies.

Chapter 2

Mechanical Quality Factor of a Beam

The mechanical quality factor of a resonator is a measure of fractional energy lost per radian of oscillation- the rate at which kinetic and potential energy are converted to some other form of (irrecoverable) energy. If the system is driven with a forcing function, the same amount of energy per radian must be supplied to maintain a steady state oscillation. If the system is resonating freely, decaying amplitude will result (shown in Figure 2.1). Equivalently, the quality factor is also a measure of the how sensitive the amplitude of vibration is to changes in the driving frequency. Therefore, we have two ways to measure the quality factor of a device: we may measure its amplitude response to a varying sinusoidal driving force, or we may perform a ring down experiment. In the latter case, a steady state oscillation is achieved, the driving force is removed, and a measurement is taken of the decaying amplitude of the vibration.

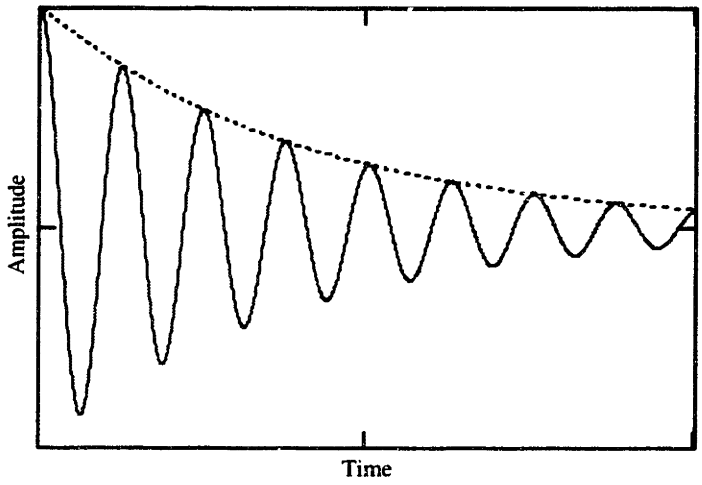

Figure 2.1: Example of a decaying sinusoid- the dashed line represents the exponential decay envelope

The equation describing the motion of the damped oscillator shown in Figure 2.1 is seen to be the product of a sinusoid and a decaying exponential:

(2.1) $x(t) = x_o \cos(\omega t) \cdot e^{-\delta t}$

$x(t)$ = Position as a function of time

x_o = Amplitude of vibration

ω = Angular frequency of oscillation $\approx \omega_o$

ω_o = The resonant angular frequency of the system with no damping

δ = Damping parameter

For systems with small damping (δ □ ω), ω is very close to the undamped resonant frequency of the system. In this chapter the assumption is made that they are approximately equal.

The quality factor is explicitly defined here as the ratio of the total (instantaneous) energy of the oscillator (kinetic plus potential) to the (instantaneous) energy dissipated per radian:

$$(2.2) \quad Q = \frac{E_{total}}{E_{lost \cdot per \cdot radian}}$$

It is shown in Appendix 1 that equation 2.2 is equivalent to the ratio of the resonant frequency ω_o and the damping parameter δ in equation 2.1 (with a factor of two):

$$(2.3) \quad Q = \frac{E_{total}}{E_{lost \cdot per \cdot radian}} = \frac{\omega_o}{2\delta}$$

In a weakly damped forced system, the amplitude of the oscillation is a function of the difference of the forcing frequency and the resonant frequency. The amplitude of vibration will peak near the resonance frequency, and a measure of the width of the peak at half of the maximum amplitude is related to the quality factor (see Appendix 1):

$$(2.4) \quad Q = \frac{E_{total}}{E_{lost \cdot per \cdot radian}} = \frac{\omega_o}{\Delta\omega}$$

$\Delta\omega$ = Width of peak at half maximum

Many of the dynamic MEMS structures incorporate beam elements into the device design: they are readily formed by standard processing techniques and they have predictable mechanical behavior. The flexible nature of these elements is exploited in sensing applications, as various techniques involve a measure of a shift in the frequency of oscillation[1]. The equation for the fundamental frequency of a beam in a flexural mode is given in equation 2.5, and a diagram of a representative vibrating beam is shown in

[1] The shift in frequency may be related to a change in the axial stress of the beam (which may be caused by an inertial force) or a change in the mass of the beam (caused by adsorption of a chemical species) as two examples of sensing applications.

Figure 2.2. A beam with two clamped ends is shown, but equation 2.5 is also valid for a beam fixed at only one end.

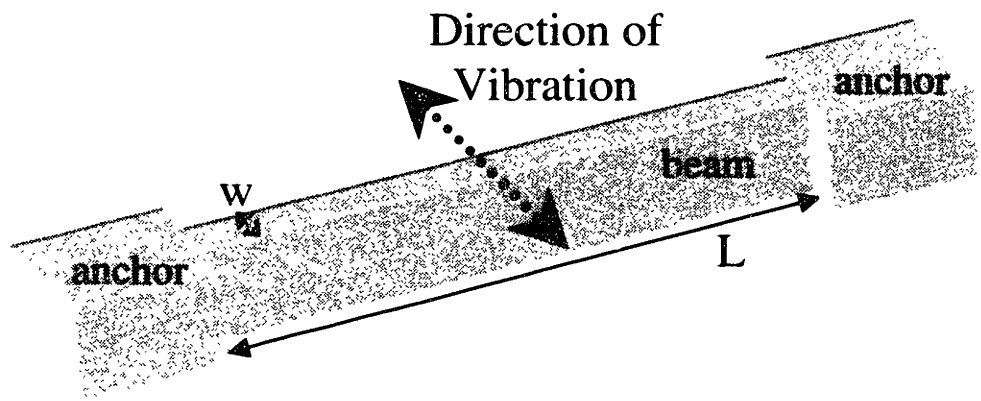

Figure 2.2: Diagram of a Vibrating Beam Element

$$(2.5) \quad \omega_n = \sqrt{\frac{EI}{\rho A}} \frac{a_n^2}{L^2} = \sqrt{\frac{E}{12\rho}} \frac{w}{L^2} a_n^2$$

ω_n = Resonant angular frequency of the fundamental mode of a beam

E = Young's modulus of the material along the longitudinal axis

I = Moment of inertia about the longitudinal axis

($I = \frac{w^3 h}{12}$ for a beam of rectangular cross section, h = beam height)

ρ = Density of beam material

A = Area of the cross section of the beam

w = Width of the beam, measured in direction of vibration

L = Length of the beam along the longitudinal axis

a_n = A constant determined by the boundary conditions

(a_n = 4.730 for a beam, 1.875 for a cantilever)

The quality factor of a micromachined silicon beam may be determined through capacitive excitation and sensing: with the silicon beam acting as one side of a charged capacitor, electrodes placed near the beam may induce movement and measure displacement. This measurement of quality factor requires integrating electrical readout circuits, and the silicon beam must be doped to give the desired electrical properties. Optical detection techniques, such as laser Doppler vibrometry, offer an alternative method of measuring displacement [6].

Chapter 3

Draper Gyroscopes

3.1 Device operation

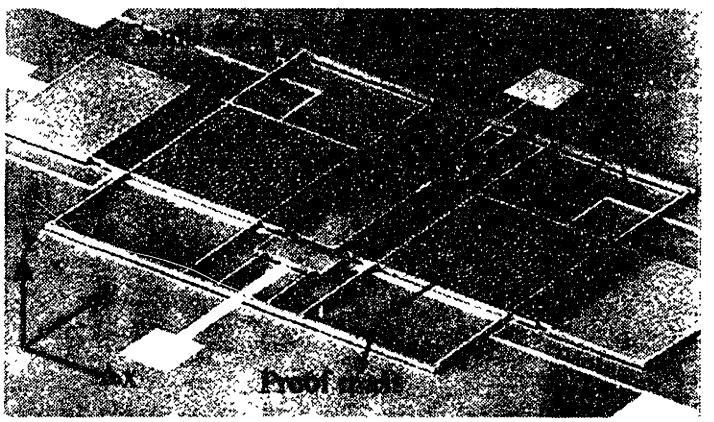

Figure 3.1: Draper Gyroscope

Figure 3.1 shows the layout of a Draper gyroscope, with salient features noted. Square pads (lighter in color) surrounding the device are electrodes. Not seen explicitly are two large electrodes under the proof masses that are used to detect out of plane motion. The large square that defines the central geometry is approximately one millimeter on a side.

The two proof masses in the picture are driven out of phase in the plane of the substrate in the x direction by the outer comb drives. The inner comb structures are used for sensing motion of the proof mass in the x direction. Each outer comb drive consists of interdigitated silicon fingers that form two electrodes. With the proof masses grounded, a time varying voltage is applied to the stationary outer electrodes, setting the proof masses in motion through an attractive capacitive force. Restoring forces are generated by the elastic support beams. Since the force between the two electrodes is proportional to the voltage squared, a DC offset is used to generate motion at the same frequency as the voltage, given by equations 3.1-3.3:

(3.1) $F = KV^2$

F = Force acting upon the proof mass from the comb drive

K = A constant of the capacitor

V = Voltage applied to the comb drive

If the voltage input is given by:

(3.2) $V(t) = V_{DC} + V_{AC}\sin(\omega t)$

The force generated on each proof mass is:

$$F = \frac{1}{2}V^2\frac{dC}{dx} = \frac{1}{2}\frac{dC}{dx}[V_{DC} + V_{AC}\sin(\omega t)]^2 = \frac{1}{2}\frac{dC}{dx}[{V_{DC}}^2 + 2V_{DC}V_{AC}\sin(\omega t) + {V_{AC}}^2\sin^2(\omega t)]$$

Using the trigonometric relationship: $\sin^2(\omega t) = \frac{1-\cos(2\omega t)}{2}$:

(3.3) $$F = \frac{1}{2}\frac{dC}{dx}\left\{{V_{DC}}^2 + 2V_{DC}V_{AC}\sin(\omega t) + {V_{AC}}^2\left[\frac{1-\cos(2\omega t)}{2}\right]\right\}$$

It is seen that this voltage signal generates a force at the voltage input frequency, as well as twice the input frequency. The input frequency is chosen to force the oscillator at the desired resonance mode.

In this manner of operation the masses will be pushed in the z direction if there is a rotation about the y-axis. The force on each proof mass is proportional to the angular velocity about the y-axis and the linear velocity in the x direction, given by the relation:

(3.4) $\vec{F} = m\vec{a}_{coriolis} = 2m(\vec{\Omega}\times\vec{v})$

F = Force on the proof mass

m = Mass of the proof mass

$\vec{a}_{coriolis}$ = Acceleration of the proof mass with respect to the frame of the gyroscope

$\vec{\Omega}$ = Angular rotation of the gyroscope with respect to inertial space

$\vec{v}$ = Velocity of the proof mass with respect to the frame of the gyroscope

The motion of the proof masses in the z direction can be determined by measuring the current output from the proof masses- if a constant voltage is maintained between the proof mass and the electrode under each proof mass, the change in gap distance will result in a change of capacitance, which will require charge be moved on or off the masses to maintain a constant voltage. The proof mass-electrode system is modeled as a pair of parallel plate capacitors:

$Q = CV_B$ = Charge on parallel plates

$C = \frac{A\varepsilon_o}{D}$ = Capacitance of parallel plates, D is a function of time

V_B = Bias voltage between the proof mass and electrode

A = Effective area of the electrodes

ε_o = Permittivity of free space

The current from the capacitor is defined as the time rate of change of the charge:

$$I = \frac{dQ}{dt} = \frac{d}{dt} CV_B = V_B \frac{dC}{dt} = V_B \frac{d}{dt}\left(\frac{A\varepsilon_o}{D}\right)$$

Let $D(t) = D_o + \Delta(t)$, it is assumed that $\Delta \ll D$

Δ = Change in distance from equilibrium

D_o = Equilibrium gap size

The current is now seen to be proportional to the velocity of the proof mass:

$$(3.5) \quad I = V_B A\varepsilon_o \frac{d}{dt}\frac{1}{D} \approx \frac{-V_B A\varepsilon_o}{D_o^2}\frac{dD}{dt} \rightarrow \frac{-V_B A\varepsilon_o}{D^2}\frac{d\Delta}{dt}$$

The current is converted to a voltage signal through the use of an integrator circuit, which gives a voltage output proportional to the position of the proof mass. It is desirable to have the integrator circuit in close proximity to the gyroscope, as the currents generated are small and may be easily dissipated. Figure 3.2 shows an electrical schematic of an integrator circuit.

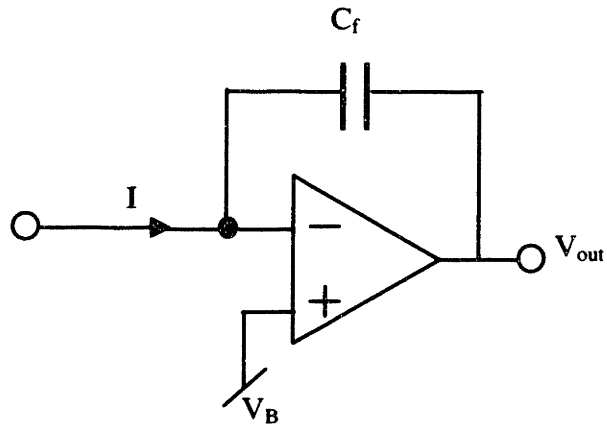

Figure 3.2: Schematic of an integrator circuit

C_f = Feedback capacitor

I = Current from proof mass

V_{out} = Voltage readout

V_B = Voltage bias on the electrode

$$\text{Here } V_{out} = \frac{1}{C_f}\int I dt \text{, so } V_{out} = \frac{1}{C_f}\int \frac{-V_B A\varepsilon_o}{D^2}\frac{d\Delta}{dt}dt = \frac{-V_B A\varepsilon_o}{C_f D^2}\int d\Delta = \frac{-V_B A\varepsilon_o}{C_f D^2}\Delta$$

In the operation of Draper's gyroscope, the masses are grounded and the electrodes underneath the two proof masses are oppositely biased. In this mode of measurement, common out of plane motion of the masses with respect to the substrate is

rejected, while differential motion relative to the substrate causes the currents from both proof masses to add constructively. This output signal constitutes a measurement of the angular rate of rotation about one axis of the device. The full electrical schematic for the gyroscope is shown in Figure 3.3.

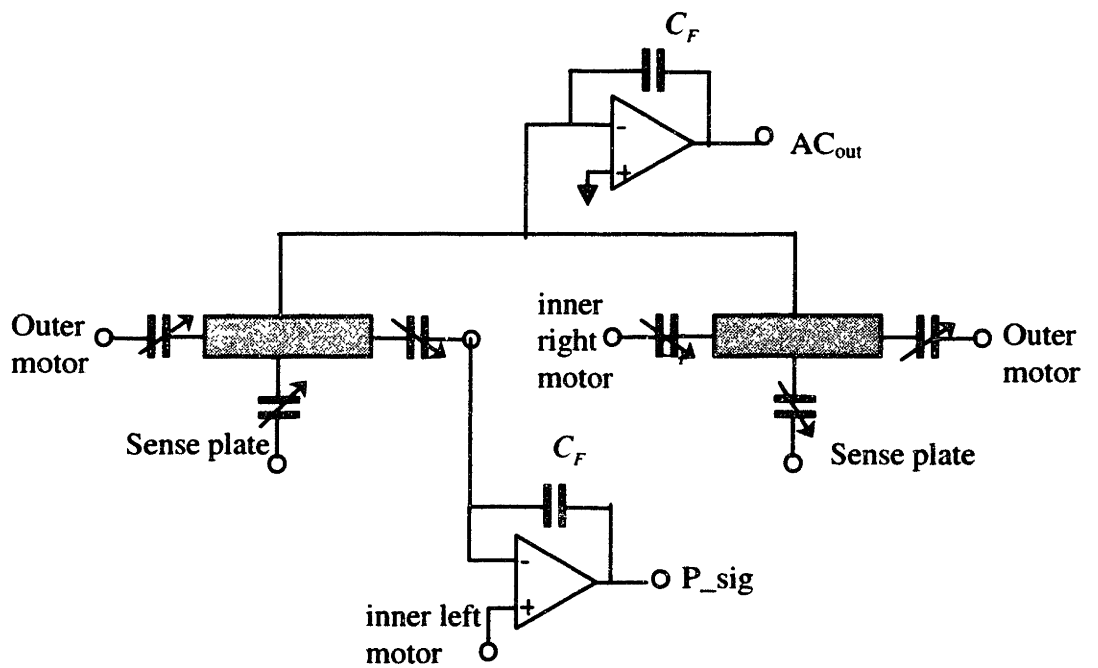

Figure 3.3: Electrical schematic of the gyroscope- proof masses are shown in gray

A similar capacitive measurement from the inner comb electrodes produces a voltage proportional to the displacement of the proof mass in the x direction. This is useful for measurements of the quality factors of the gyroscopes oscillating in this sensing mode. Unfortunately, limitations in our experimental setup prevented this voltage signal from being used. To generate a signal proportional to the displacement in the x direction, a carrier signal is used to isolate the desired signal. The carrier is placed on the inner comb drive and is used to demodulate the output from the integrator circuit coming from the proof mass.

3.2 Device Construction

Device layers were grown on silicon substrates for four of the five different materials used for making the gyroscopes in this study. All four were grown with high concentrations of boron (greater than 10^{20} cm^{-3}) and varying concentrations of germanium (0, 2, 23, 30%)[2]. For the fifth material, boron was diffused into the top layer of the substrate to a boron concentration similar to that of the other materials. Etch processes on the top layer of the doped silicon defined the device geometry, which were anodically bonded (device layer down) to metal-patterned glass substrates. The undoped regions of the silicon substrates were thinned back to the device layer and the device parts were released.

Although all the gyroscopes made from the different materials were of similar design scale, the dimensions of the beams varied slightly from material to material due to variations in processing the different materials.

[2] The 23% and 30% germanium compositions were custom epitaxial films provided generously by collaborator Matt Currie in Professor Fitzgerald's laboratory.

Chapter 4

Q Measurements and Results

4.1 Experimental setup

Measurements of the quality factors of Draper's gyroscopes were made at the wafer level inside a vacuum probe station. The frequency of the forcing voltage on the outer comb drive for one proof mass was swept up in frequency about the desired resonance mode and compared to the demodulated output voltage from the proof masses. Quality factor measurements were performed by measuring the frequency bandwidth at half the maximum output voltage (Appendix 1).

Figure 4.1 is a schematic of the test setup. The sweep frequency is generated by the Hewlett Packard 3562A signal analyzer. The carrier signal is generated by the Hewlett Packard 3310A signal generator. These signals are routed through a test box, which sends all input and output signals to the vacuum-enclosed gyroscope through a single shielded cable. Also enclosed in the vacuum chamber are the preamplifiers needed for the gyroscope outputs. These need to be located close to the readout nodes, and so they are integrated onto the face of the probe card. The amplified gyroscope outputs are routed back through the test box, where they can be demodulated and fed back into the 3562A spectrum analyzer. The oscilloscope is used for a reference, to monitor the gyroscope signal before demodulation (labeled AC out).

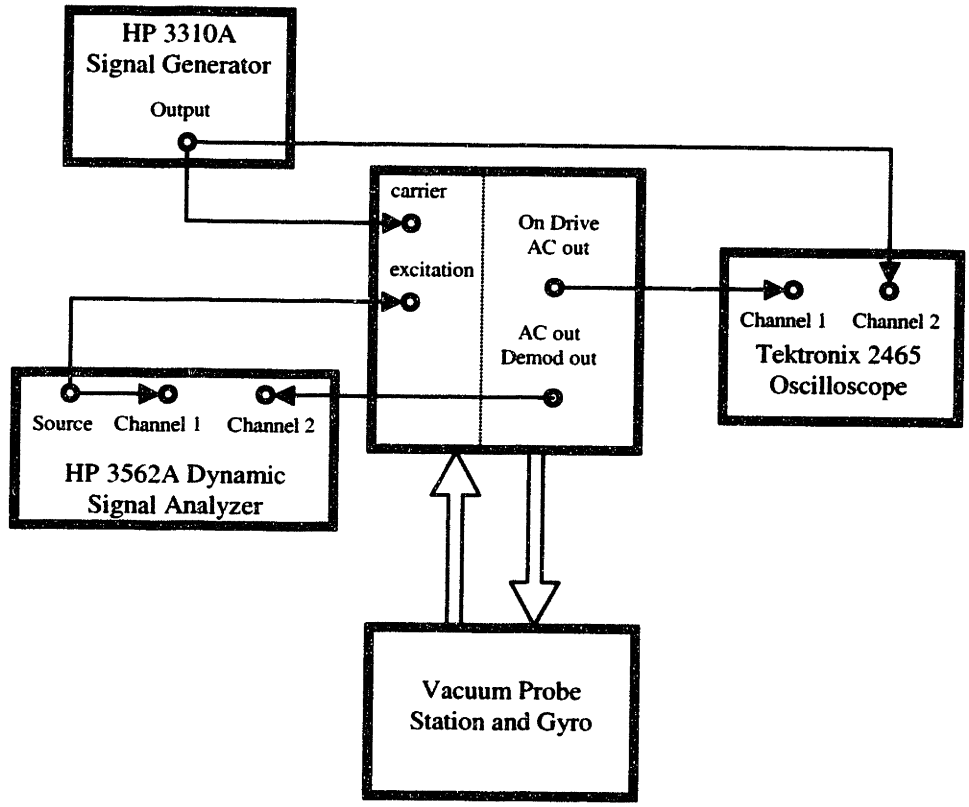

Figure 4.1: Quality Factor Test Setup

4.2 Experimental Procedure

Once the test device wafer is placed on the test platform inside the vacuum chamber, the chamber is sealed and pumped down to approximately 1 mTorr. This step is taken to minimize the effects of fluidic damping. All the electronics are turned on for at least fifteen minutes prior to any measurements being taken; this allows the amplifiers inside the vacuum chamber to stabilize. (The performance of the amplifiers was noted to drift as they warmed up- the vacuum conditions prevented them from conducting heat away as efficiently as they would at atmospheric conditions.) Next the probe card tips are brought into contact with a test device after aligning the device's electrical test pads with the contact tips of the probe card. This step is performed by visual inspection through a

port in the top of the vacuum chamber- adjustments to the relative position are made by adjustment of the wafer stage through position controllers on the outside of the chamber.

A Hewlett-Packard 3310 Signal Generator was used to provide a 100kHz, 300 mV (peak to peak) carrier signal that was routed to the right inner motor. A Hewlett-Packard 3562A Dynamic Signal Analyzer provided a 50mV (peak to peak) sweeping frequency to the outer comb drives to provide the proof mass forcing voltages. Both outer motors were biased at +5V (in addition to the AC forcing voltage), the left inner motor was biased to +5V, the electrodes under the proof mass were grounded, and the proof masses themselves were grounded. (All voltage biases were provided with a power supply routed through the electronics box.)

Once the resonant mode of interest for a particular gyroscope was identified, one of two frequency scans was performed. For devices with a quality factor of greater than 50,000 a 1 Hz frequency scan was performed about the resonant frequency. The spectrum analyzer was set to sample at 5mHz intervals, and average ten voltage readings at each interval. For the materials with quality factors of less than 50,000 a 5 Hz frequency scan about the peak resonance was performed, sampling at 25mHz intervals. For each of these measurements, the source signal from the spectrum analyzer is compared with the voltage signal from the proof masses (which should be proportional to the position of the masses). The ratio of the signal amplitudes and the relative phase of the signals versus the source frequency are displayed on the spectrum analyzer monitor. Once a frequency sweep is complete, the bandwidth of the peak at half maximum is measured in addition to the resonant frequency and the quality factor is calculated using equation 2.4. A sample Q measurement is shown in Figure 4.2. The circles on either side of the peak are set at the –3dB points relative to the peak maximum, and the spectrum analyzer determines the peak frequency (shown as 'F') and one half the bandwidth (shown as 'D' on the right hand side- it is displayed as negative to relate it to the damping parameter).

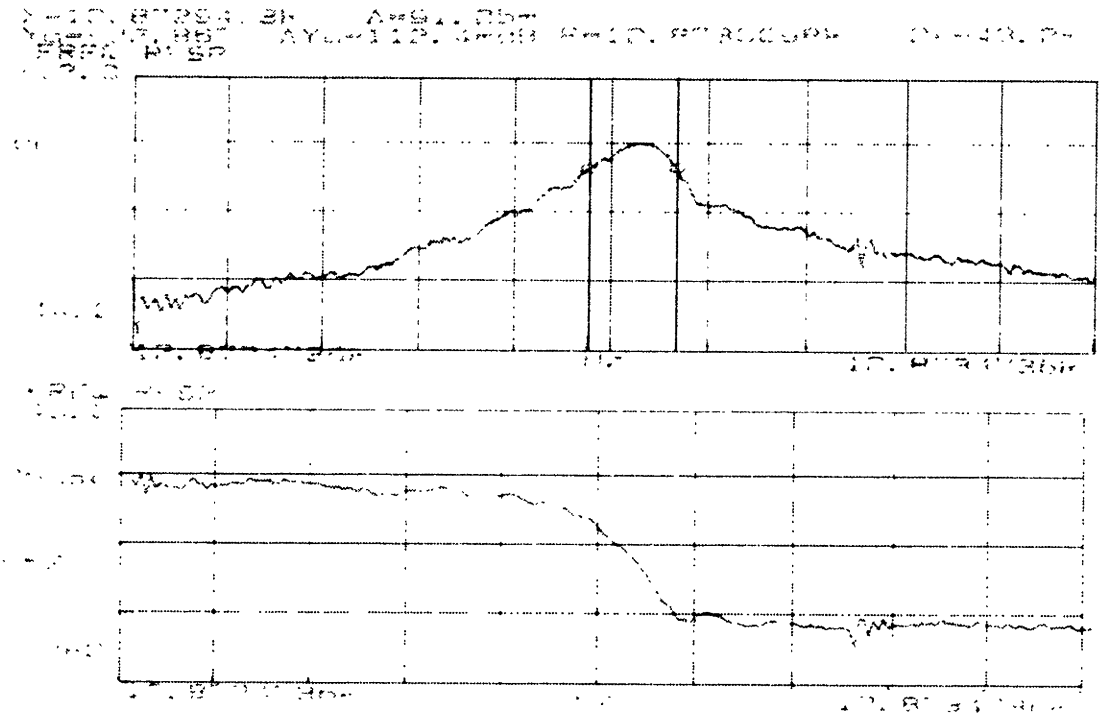

Figure 4.2: Sample quality factor measurement- the ratio of the voltage signals is plotted on top, the relative phase is shown on the bottom

4.3 Measurement Repeatability

To determine the scatter in the measured Q values, twenty Q measurements were taken on one device. The average Q was calculated to be 232,000, while the standard deviation was 4660 or 2%. For each gyroscope Q measurement, at least two measurements were taken. If these two Q values were not within 1% of each other, a third measurement was taken and the measurements were averaged to determine the reported Q of a particular gyroscope.

4.4 Experimental Results

Figure 4.1 shows the results of Q measurements for one device taken as a function of chamber pressure. This plot is shown for illustrative purposes, to demonstrate the

effect of fluidic damping upon a gyroscope's operation. At about 10mTorr of pressure the lead cause of damping shifts from fluidic damping to some other performance limiter. All the results presented in this section were taken at a pressure of 1mTorr or lower to minimize the fluidic contribution to damping. This was done to isolate the material damping mechanism for detailed study. (A gap exists in the data between 1 mTorr and 10 mTorr due to difficulties regulating the pressure.)

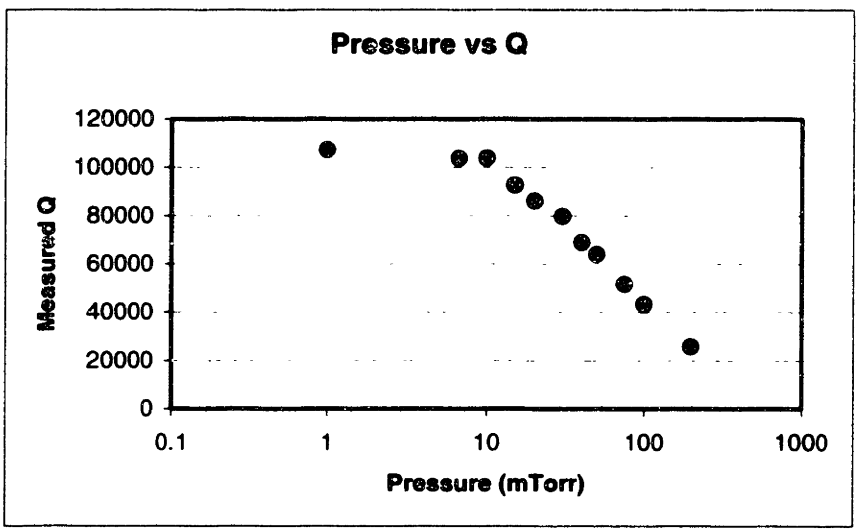

Figure 4.3: Plot of the effect of pressure on the measured Q value

The results of the measured Q values for the five different materials under study are shown in Table 4.1. Approximately ten devices were measured on each wafer, and the average frequencies and quality factors were recorded. Although the standard deviation in multiple measurements of the same device might be on the order of a few percent, the standard deviation of measurements of different devices on the same wafer can be seen to be up to twenty percent, as is the case for the boron diffused wafer. The average values of the resonant frequencies and the quality factors were tabulated in an effort to understand the immediate concern that the devices with a higher germanium concentration have lower average Q values.

	SiB epi	SiGeB 2%	SiGeB 23%	SiGeB 30%	B-diff
Devices Tested	9	9	9	10	10
Average frequency	12851	13327	10357	10785	12361
Average Q	177,000	62,800	27,100	23,400	219,000
Q standard deviation	10%	18%	6%	10%	20%

Table 4.1: Results of the Q tests for different silicon alloys

Chapter 5

Effect of Thermoelastic Damping on Measured Q

The gyroscopes produced at Draper Laboratory have high concentrations ($\sim 10^{20}/cm^3$) of boron incorporated into the silicon lattice to enhance the electrical conductivity of the base silicon material. The boron serves to increase the number of charge carriers on the proof masses, which is necessary to generate good current signals from the proof masses during operation. The 2% Ge SiGeB material has germanium added to the silicon/boron lattice to help offset the lattice strain in the epitaxial layer introduced by the high boron concentration. The resulting devices built from this material exhibit less curvature and better build precision than those built from SiB. However, it was noticed that the introduction of germanium had a deleterious effect on the measured quality factor. Devices built from wafers with higher concentrations of germanium were tested to see if the downward trend in measured Q continued. Inspection of Table 4.1 indicates that this is indeed the case.

Quantity	Units	SiB epi	SiGeB 2%	SiGeB 23%	SiGeB 30%	B-diff	Si Value	Ge Value
CTE	1/K	2.57E-06	2.65E-06	3.33E-06	3.55E-06	2.59E-06	2.56E-06	5.80E-06
reference		Si value	Int	Int	Int	[7]	[8],[9]	[9]
Elastic Modulus	N/m^2	1.69E+11	1.68E+11	1.54E+11	1.49E+11	1.69E+11	1.69E+11	1.03E+11
reference		Si value	Int	Int	Int	Si value	[9]	[9]
Density	kg/m^3	2.33E+03	2.39E+03	3.02E+03	3.24E+03	2.33E+03	2.33E+03	5.35E+03
reference		Si value	Int	Int	Int	Si value	[8]	[9]
Specific Heat	J/(K*kg)	7.00E+02	7.05E+02	6.23E+02	5.95E+02	7.00E+02	7.13E+02	3.20E+02
reference		Si value	Int	Int	Int	Si value	[10]	
Thermal Conductivity	J/(K*s*m)	80	10.67	5.71	5.52	80.00	1.56E+02	58.61
reference		[11,12]	[11,12]	[11,12]	[11,12]	[11,12]	[9],[10]	[9]

Table 5.1: Properties of the gyroscope materials – "Int" means that the property was interpolated from the pure silicon and germanium properties.

Table 5.1 contains some of the elastic and thermal properties for the materials tested. Of the parameters listed, the thermal conductivity is seen to vary most dramatically, differing by a factor of almost fifteen between the materials without germanium and the SiGeB wafer with 30% germanium. The germanium atoms are

understood to act as phonon scattering centers, greatly decreasing the thermal conductivity in the silicon lattice [13]. The fact that the thermal conductivity is greater in devices with higher quality factors suggests that the damping may be directly related to the thermal properties of the solid. Zener offered the following equation for thermoelastic damping in a beam element (vibrating in a flexural mode) in his 1937 paper "Internal Friction in Solids":

$$(5.1) \quad \frac{1}{Q_{TED}} = \frac{E\alpha^2 T_o}{c_\sigma \rho} \frac{\omega\tau_z}{1+(\omega\tau_z)^2}$$

E = Elastic modulus

α = Coefficient of thermal expansion

T_o = Initial temperature

c_p = Specific heat capacity, at constant pressure

ρ = Density

The quality factor of a beam element (undergoing thermoelastic dissipation) is proportional to a damping factor containing thermal and elastic material parameters, and a frequency function that contains a relaxation time that is proportional to the thermal diffusivity and the width of the beam:

$\tau_z = \frac{b^2}{\pi^2 \chi}$ = Relaxation time consant

$\chi = \frac{\kappa}{c_p \rho}$ = Thermal diffusivity

b = Beam width, as measured in direction of flexural displacement

κ = Thermal conductivity

As was mentioned in Chapter 3, the proof mass support beams provide the restoring forces on the proof masses. As the proof masses are displaced from equilibrium, each one of the four support beams may be thought of as one half of a beam twice its length vibrating in the lowest flexural mode. Using expression 5.1, along with measured beam widths and resonant frequencies, the contribution to the quality factor from thermoelastic dissipation is calculated for the five wafers is this study. The results are shown in Table 5.2.

Quantity	Units	SiB epi	SiGeB 2%	SiGeB 23%	SiGeB 30%	B-diff
Relaxation Time Constant	s	9.00E-08	7.62E-07	1.40E-06	1.54E-06	7.44E-08
Beam Width	m	6.60E-06	6.90E-06	6.48E-06	6.60E-06	6.00E-06
Resonant Frequency	Hz	12,851	13,327	10,357	10,785	12,361
Thermoelastic Q value		670,000	74,800	40,700	33,000	829,000

Table 5.2: Calculated contributions to the quality factor from thermoelastic damping

The thermoelastic damping values listed in Table 5.2 predict the correct relative order of the measured Q values for the different wafer materials, but all the Q values in Table 5.2 are higher than what is observed experimentally. This difference in Q values may be explained by other forms of damping that are taking place. Unaccounted for are damping losses caused by anelastic anchors, power loss through proof mass current dissipation in the operational amplifier[3], residual fluidic damping, and possibly other anelastic mechanisms within the structure, such as dislocation or point defect motion. Each of these mechanisms has its own associated Q value, and the expression for the overall Q is (Appendix 1):

$$\frac{1}{Q_{total}} = \frac{1}{Q_{TED}} + \frac{1}{Q_{anchor}} + \frac{1}{Q_{fluid}} + \frac{1}{Q_{electrical}} + \ldots$$

[3] A calculation was done of the contribution due to the electrical power dissipation. It turns out to predict a Q value in the billions, and is the same for all devices measured. It is therefore negligible in this investigation.

If the assumption is made that all the damping mechanisms besides thermoelastic damping are similar between the different wafers, we may write the following expression for the measured Q value:

$$\frac{1}{Q_{total}} = \frac{1}{Q_{TED}} + \frac{1}{Q_{other}} \tag{5.2}$$

When a value of $Q_{other} = 250,000$ is used, it is found that equation 5.2 yields Q values that are in reasonable agreement with experiment. The calculated and observed values are compared in Figure 5.1.

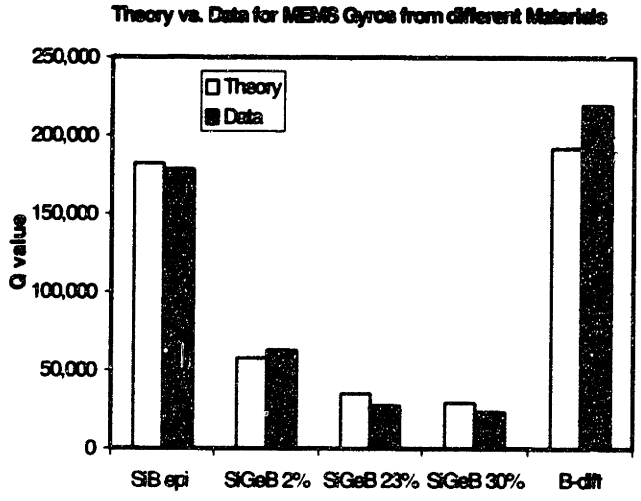

Figure 5.1: Measured Q values versus theory

The fact that the Q_{other} term may be similar between the different materials is interesting, and may lead to further improvements in device design. However, the number is significant in the respect that three of the devices are limited in performance by thermoelastic damping, having lower Q_{TED} terms than Q_{other}. Adding germanium to offset lattice strain appears to have an adverse effect on quality factor[4]. The calculation for thermoelastic damping was straightforward for the gyroscopes used for this study, but as more complicated designs are introduced the analytical equation for beams will be of

[4] It is interesting to note that according to equation 5.1, at much higher frequencies of operation, decreasing the thermal conductivity will result in a reduction of thermoelastic damping.

little use. It is this observation that motivated the development of a finite element model to evaluate thermoelastic damping in micromachined structures.

Section 2

The purpose of this section is to present the theory of thermoelastic damping, and show the steps that were taken to translate the governing equations into a finite element model. The finite element model is validated through a comparison to analytical solutions for a simple beam, and then used to determine the damping in more complicated geometries.

Chapter 6

Anelasticity and Anelastic Damping

Stresses applied to a perfectly elastic material will result in an instantaneous equilibrium strain state, by definition. Anelasticity departs from elastic behavior in the respect that an equilibrium strain state is approached only after a passage of time. (For both materials the removal of the applied stress results in complete recovery of the initial state, and in this manner both differ from a viscoelastic material.) While for an elastic material the elastic modulus is a time-independent constant for a given material, an anelastic material displays an elastic modulus that is dependent upon time. This time dependent modulus may be thought of as consisting of two parts: one that describes the instantaneous deformation (the elastic part) and one that describes the anelastic deformation (a constant multiplied by some function of time). For a constant applied stress, the time-dependent strain is given by the equation[5]:

$$(6.1) \quad \varepsilon(t) = \frac{\sigma}{E(t)}$$

$\varepsilon(t)$ = Strain as a function of time

σ = Constant applied stress

[5] Only one directional component of stress and strain is included in these equations, for simplicity.

The expression for the time dependent modulus is:

$$(6.2) \quad E(t) = E_R - \delta E[1 - \exp(-\frac{t}{\tau_\sigma})], \text{ where } E_U = E_R + \delta E$$

The bounds on the modulus are the unrelaxed and relaxed moduli.

E_R = Relaxed Young's modulus (modulus as $t \to \infty$)

E_U = Unrelaxed Young's modulus (modulus at $t = 0$)

δE = Difference between the relaxed and unrelaxed Young's modulus ($\delta E > 0$)

τ_σ = Relaxation time constant, associated with constant stress measurement

The general equation for the anelastic response of a material, where both stress and strain are functions of time, is given by:

$$(6.3) \quad \sigma + \tau_\varepsilon \frac{d\sigma}{dt} = E_R(\varepsilon + \tau_\sigma \frac{d\varepsilon}{dt})$$

τ_ε = Relaxation time constant, associated with constant strain measurement

The fact that it takes some finite amount of time for the material to approach an equilibrium state for some applied stress is significant in systems with time varying loads, as it may result in damping behavior. This can be shown with a work integral of the oscillatory motion. The energy lost in one radian is calculated by the work done to maintain the oscillation:

$$(6.4) \quad \Delta W = \frac{1}{2\pi} \oint_{one\text{-}cycle} \sigma d\varepsilon$$

It is not proven here, but it is reasonable to assume that an applied sinusoidal stress will result in a sinusoidal strain, whose frequency is the same as the applied stress, but possibly shifted by a phase angle:

(6.5a) $\sigma(t) = \sigma_o \cos(\omega t)$

(6.5b) $\varepsilon(t) = \varepsilon_o \cos(\omega t - \phi)$

Here σ_o and ε_o are taken to be real, and ϕ is taken be to be positive, meaning that the stress leads the strain. To estimate the energy lost in terms of the applied strain, ε_o may be written in terms of the stress and the relaxed elastic modulus:[6]

(6.6) $\varepsilon_o = \frac{\sigma_o}{E}$

The integral becomes: $\Delta W = \frac{1}{2\pi} \int_0^{2\pi} \frac{-\sigma_o^{\,2}}{E} \cos(\omega t) \sin(\omega t - \phi) d(\omega t)$

Carrying out the integration, an expression is derived for the energy lost per radian:

(6.7) $\Delta W = \frac{\sigma_o^{\,2}}{2E} \sin(\phi)$

To find the fractional energy lost, this value is compared with that of the total amount of stored energy, which is obtained by an integral of the stress applied to the material from zero to the maximum strain:

(6.8) $\Delta W = \int_0^{\pi/2} \sigma d\varepsilon$

[6] This substitution can be made assuming that the difference between the relaxed and unrelaxed moduli is small, which is a reasonable assumption for certain damping mechanisms, such as thermoelastic dissipation in silicon.

Carrying through the integration:

$$(6.9)\quad \Delta W = \frac{\sigma_o^{\,2}}{2E}\cos(\phi) + \left(\frac{\pi}{2}\right)\frac{\sigma_o^{\,2}}{2E}\sin(\phi)$$

The first term on the right hand side is the maximum energy stored, the second term is the energy dissipated in the $\frac{\pi}{2}$ radians in the integration.

The ratio of the energy lost per radian to the maximum stored energy is:

$$(6.10)\quad \frac{\Delta W}{W} = \frac{\frac{\sigma_o^{\,2}}{2E}\sin(\phi)}{\frac{\sigma_o^{\,2}}{2E}\cos(\phi)} = \tan(\phi)$$

At this point it is useful to identify the equivalence between equation 6.10 and 2.2:

$$\frac{\Delta W}{W} = \frac{E_{lost\cdot per\cdot radian}}{E_{total}} = \frac{1}{Q_{anelastic}} = \tan(\phi)$$

Determining the phase angle φ determines the quality factor of a resonator experiencing anelastic damping. To determine φ, the complex representations of stress and strain may be substituted into equation 6.3.

$$(6.11)\quad \sigma(t) = \sigma_o e^{i\omega t} \text{ and } \varepsilon(t) = \varepsilon_o e^{i(\omega t - \phi)}$$

Now the modulus can be expressed as a complex quantity:

$$(6.12)\quad E = \frac{\sigma}{\varepsilon} = \frac{\sigma_0 e^{i\omega t}}{\varepsilon_0 e^{i(\omega t - \delta)}} = \frac{\sigma_0}{\varepsilon_0} e^{i\delta}$$

The ratio of ε_o to σ_o is not constant, but depends upon the frequency of oscillation and the phase angle. Substituting the expressions of stress and strain into 6.3, the ratio of ε_o to σ_o and the phase angle can be determined. (The equation 6.3 can be broken into two equations- real and imaginary- that can be solved to yield the two values.)

The expression for the phase angle is:

$$(6.13)\quad \tan(\phi) = \frac{\omega(\tau_\sigma - \tau_\varepsilon)}{1 + \omega^2 \tau_\sigma \tau_\varepsilon}$$

Making the substitution:

$$(6.14)\quad \tau = \sqrt{\tau_\varepsilon \tau_\sigma}$$

Gives the expression:

$$(6.15)\quad \tan(\phi) = \left[\frac{(\tau_\sigma - \tau_\varepsilon)}{\sqrt{\tau_\sigma \tau_\varepsilon}} \right] \cdot \frac{\omega\tau}{1 + (\omega\tau)^2}$$

Which can be represented as the product of a constant of the material multiplied by a function of frequency:

$$\tan(\phi) = \Delta \cdot f(\omega)$$

$$\Delta = \frac{(\tau_\sigma - \tau_\varepsilon)}{\sqrt{\tau_\sigma \tau_\varepsilon}} = \text{Relaxation strength of the modulus}$$

These relaxation time constants may be related to the relaxed and unrelaxed moduli as follows:

From reference [3]:

$$(6.16)\quad E_U = E_R \frac{\tau_\sigma}{\tau_\varepsilon}$$

So the relaxation strength is:

$$(6.17)\quad \Delta = \frac{(\tau_\sigma - \tau_\varepsilon)}{\sqrt{\tau_\sigma \tau_\varepsilon}} = \frac{E_U - E_R}{\sqrt{E_U E_R}}$$

The expression for the quality factor is now:

$$(6.18)\quad \frac{1}{Q_{anelastic}} = \Delta \frac{\omega\tau}{1+(\omega\tau)^2}$$

The frequency response is given by the expression:

$$(6.19)\quad f(\omega) = \frac{\omega\tau}{1+(\omega\tau)^2}$$

It can be seen that the function of frequency has the following high/low freq dependence:

If $\omega\tau << 1, f(\omega) \to \omega\tau$

If $\omega\tau >> 1, f(\omega) \to \frac{1}{\omega\tau}$

$f(\omega)$ is greatest when $\omega\tau = 1$, the peak damping frequency: $\omega_p = \frac{1}{\tau}$

This peak is known as a Debye relaxation peak, and is shown in Figure 6.1.

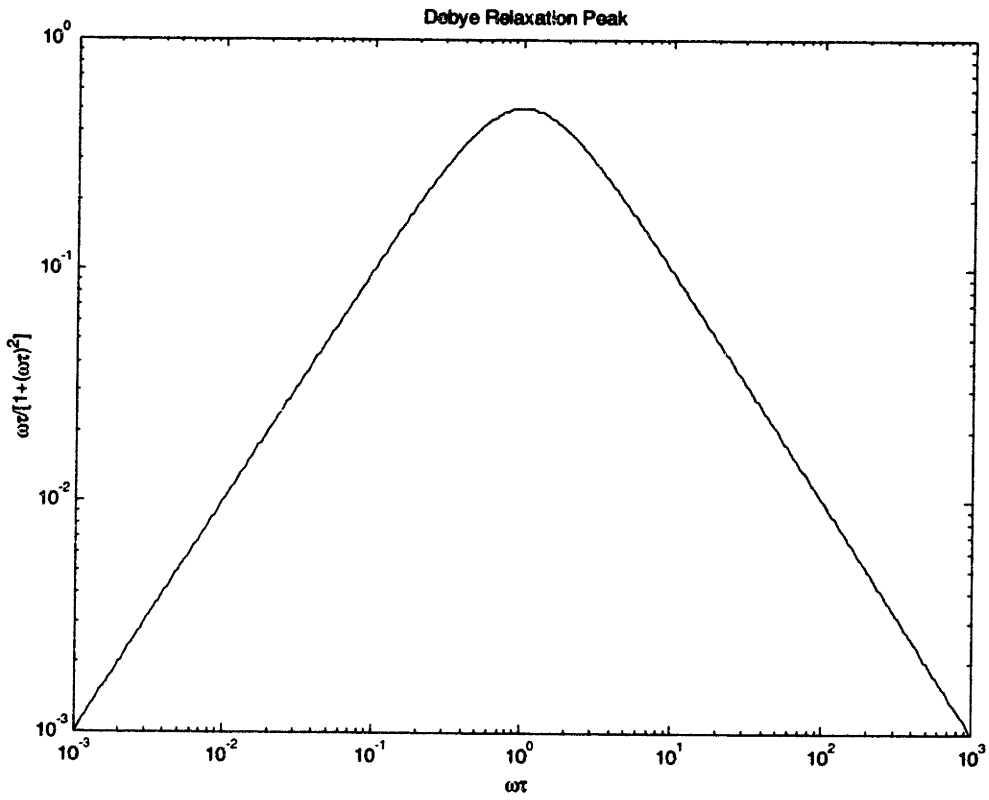

Figure 6.1 Debye Relaxation peak (relaxation strength equals one)

The values of the unrelaxed and relaxed moduli as well as the relaxation time constant τ are governed by internal parameters that are measures of the state of the material. To determine the value of the relaxation strength, the contributions to the elastic modulus must be identified. Any change in internal structure will result in a change in the elastic modulus. For example, application of stress to a material may change the equilibrium point defect density, which in turn alters the elastic modulus. The elastic modulus may also be affected even if the crystal structure is unchanged, as in the case of uniform expansion of the material. An expression for the total quality factor due to anelastic damping may be written as the sum of these individual anelastic damping contributions:

$$\frac{\sum E_{lost\cdot per\cdot radian}}{E_{total}} = \sum \frac{1}{Q_{anelastic}} = \frac{1}{Q_{total\cdot anelastic}} \tag{6.20}$$

In general, these different damping mechanisms will have different associated relaxation strengths and peak damping frequencies. In addition, certain damping mechanisms (such as dislocation movement) may have broader peaks, reflecting the different mobilities of the different individual dislocations. Although there may be many possible different contributions to the anelastic behavior of a material, it is possible that one damping mechanism dominates the anelastic response for a particular operating frequency. Determining what loss mechanism dominates in a particular system will involve calculations of the relaxation strengths and relaxation time constants for all the known possible damping mechanisms. This is in reality not a trivial task, as many of the numbers needed for these calculations may not be known for a particular material (such as the point defect density in a silicon based device after processing) or may be dependent upon the geometry of the oscillator, in which case a closed formed solution may not exist. In these cases approximations or even (informed) guesses may need to be made.

Equally important in developing an understanding of the damping behavior of an oscillator is the identification of external damping mechanisms. Some of the important contributors to damping in micro-electromechanical systems are fluidic losses associated with transfer of kinetic energy to the surrounding medium (air), transfer of kinetic and potential (elastic) energy to the support structure of the device, conversion of kinetic and potential energy to heat (which may then be radiated or conducted away), and losses associated with coupling of the motion to the electrical subsystem (in the case of a capacitive device). The total quality factor for the oscillator is now a sum of the contributions to internal and external damping:

$$\frac{1}{Q_{total}} = \frac{1}{Q_{anelastic}} + \frac{1}{Q_{fluidic\ loss}} + \frac{1}{Q_{anchor\ loss}} + \ldots$$

To improve the performance of a damped oscillator, the leading contribution to damping must be identified and minimized. Since both internal damping and external damping are a function of the geometry of the device, it would be ideal to develop

models that evaluate the contribution of the leading damping mechanisms for different geometries. Finite element analysis is a tool that is useful for numerical evaluation of physical equations over complex geometries, and offers a way to accomplish this goal.

Chapter 7

Thermoelasticity Theory

7.1 Overview

A material in thermal and mechanical equilibrium subjected to an inhomogeneous stress state (such as that of a beam during flexural displacement) will develop a nonuniform temperature field, if the deformation occurs without any heat transport. This condition will exist when the stress state is applied on a time scale that is very short compared to the amount of time it would take for the material to reach thermal equilibrium. Alternately, the stress state may be imposed so slowly such that the material is in constant thermal equilibrium. A general measure of the 'time to reach thermal equilibrium' can be understood as a relation between the thermal diffusivity of the material and the distance between the regions of different temperature (diffusion length).

(7.1) $l = \sqrt{D\tau}$

l = Diffusion length
D = Diffusivity
τ = Relaxation time

The thermal diffusivity (here represented by the symbol χ) is defined as the ratio of the thermal conductivity and the volumetric heat capacity.

(7.2) $\chi = \frac{\kappa}{c_p \rho}$

Thermoelastic dissipation occurs in a material when the time scale of the imposed stress is of the magnitude of the thermal relaxation time. Heat flow between regions of

different temperature occurs irreversibly, and energy stored elastically in the material is converted to heat. It is evident that to avoid thermal elastic dissipation occurring in oscillatory structures, they be must operated at periods different than their associated thermal relaxation times. The frequency dependent damping behavior may be described by equation 7.3 (as derived in Chapter 6):

$$(7.3) \quad \frac{1}{Q_{anelastic}} = \Delta \frac{\omega\tau}{1+(\omega\tau)^2}$$

$$(7.4) \quad \Delta = \frac{E_U - E_R}{\sqrt{E_U E_R}}$$

$$(7.5) \quad E_U = \left(\frac{\partial\sigma}{\partial\varepsilon}\right)_S, \quad E_R = \left(\frac{\partial\sigma}{\partial\varepsilon}\right)_T$$

The magnitude of the relaxation strength is a measure of the fractional difference of the relaxed and the unrelaxed elastic moduli, which are interpreted here as the isothermal and the adiabatic elastic modulus, respectively. We may determine the difference by understanding the two final equilibrium strain states for the same imposed stress. The difference in the two final strain states is due to the transfer of heat with the surroundings. This transfer is necessary to equalize the change in temperature caused by the application of stress.

$$(7.6\text{ a}) \quad \sigma = E_U \varepsilon_{elastic}$$

$$(7.6\text{ b}) \quad \sigma = E_R \varepsilon_{anelastic}$$

$\varepsilon_{elastic}$ = Elastic strain

$\varepsilon_{anelastic} = \varepsilon_{elastic} + \varepsilon_{thermal}$ = Anelastic strain

$\varepsilon_{thermal} = \alpha\Delta T$ = Thermal strain

Equating equations 7.6a and 7.6b, and substituting for $\varepsilon_{anelastic}$:

(7.7) $$E_U \varepsilon_{elastic} = E_R(\varepsilon_{elastic} + \alpha \Delta T)$$

Here the expression for ΔT may be determined by the relation between the change in stress and the change in temperature, as derived in Appendix 2:

(A2.11) $$\left(\frac{\partial T}{\partial \sigma}\right)_S = -\frac{\alpha T_{init}}{c_\sigma \rho}$$

T_{init} = Initial temperature

The change in temperature the material experiences to equilibrate with its surroundings is the same as the temperature change that occurred when stressed, with the opposite sign:

$$\Delta T = -\left(\frac{\partial T}{\partial \sigma}\right)_S \Delta\sigma \rightarrow -\left(\frac{\partial T}{\partial \sigma}\right)_S \sigma$$ (Assuming the initial stress is zero)

Substituting this result into equation 7.7:

(7.8) $$E_U \varepsilon_{elastic} = E_R(\varepsilon_{elastic} + \frac{\alpha^2 T_{init}}{c_\sigma \rho}\sigma) = E_R \varepsilon_{elastic} + E_R \frac{\alpha^2 T_{init}}{c_\sigma \rho}\sigma$$

Rearrange 7.8 in terms of the difference in the moduli, and rewrite the stress in terms of the elastic strain:

(7.9) $$(E_U - E_R) = \frac{E_R \alpha^2 T_{init}}{c_\sigma \rho}\frac{\sigma}{\varepsilon_{elastic}} = \frac{E_R^2 \alpha^2 T_{init}}{c_\sigma \rho}$$

For silicon, the value of the coefficient of thermal expansion is parts per million per degree Kelvin, making the value of the difference of the magnitudes of the elastic moduli much smaller than the moduli themselves, at reasonable operating temperatures. Taking the commonly reported value of elastic modulus to mean the relaxed elastic modulus, the following approximations are made:

$$E_R \approx E$$

The denominator of the expression for the relaxation strength in equation 7.4 is approximately to:

$$\sqrt{E_U E_R} \approx E$$

The final expression for the relaxation strength, in terms of the thermal and mechanical material properties:

$$(7.10) \quad \Delta = \frac{E\alpha^2 T_{unit}}{c_\sigma \rho}$$

All that is need for the expression of the quality factor in equation 7.3 is the value of the thermal relaxation time, τ. For complicated geometries the regions of different stress may be different distances apart, but for a beam under flexural bending, there will exist regions of tension and compression at the outside edges of the beam, with the direction of the temperature gradient across the beam. Thus there is a common length associated with the varying regions of stress, and the time constant may be related to this length and the thermal diffusivity. Clarence Zener defined the relaxation time constant in his seminal paper on internal friction [1]:

$$(7.11) \quad \tau_z = \frac{b^2}{\pi^2 \chi}$$

This time constant, along with the relaxation strength given in equation 7.10 may be substituted into equation 7.3 to provide a reasonable approximation of the quality factor of a vibrating beam element experiencing thermoelastic damping:

$$(7.12)\quad \frac{1}{Q_{ted}} = \frac{E\alpha^2 T_{init}}{c_\sigma \rho} \frac{\omega\tau_z}{1+(\omega\tau_z)^2} \qquad \text{(Zener)}$$

The frequency to be used is either the resonant frequency of the beam or the frequency of the forcing function. This work was later extended in a paper written by M. L. Roukes and Ron Lifshitz [3] to provide an exact solution to the problem. The equation developed in the paper has the same form as 7.12, with a different frequency function:

$$(7.13)\quad \frac{1}{Q_{ted}} = \frac{E\alpha^2 T_{init}}{c_\sigma \rho}\left[\frac{6}{\xi^2} - \frac{6}{\xi^3}\frac{(\sinh\xi+\sin\xi)}{(\cosh\xi+\cos\xi)}\right], \quad \xi = b\sqrt{\frac{\omega}{2\chi}} \qquad \text{(Roukes)}$$

An important feature of both equation 7.12 and 7.13 is that the only beam dimension that explicitly appears in the equations is the width of the beam[7].

7.2 Coupled Equations of Thermoelasticity For an Isotropic Material

The constitutive relation for the material can be combined with force balance and energy conservation to obtain the coupled dynamics of the system.

The general elastic equation for a material is given by the following expression of force balance:

[7] These equations will be used to evaluate the accuracy of the finite element model. It is stressed that equation 7.12 is treated as an approximate solution, whereas 7.13 is regarded as exact.

(7.14) $$\frac{F_i}{V} = \frac{\partial \sigma_{ij}}{\partial x_i} = \rho \frac{\partial^2 u_i}{\partial t^2}$$

F_i = Force on a small cube of material in the direction of i (where i = x, y, or z)

V = Volume of cube

σ_{ij} = Stress on the face of the cube normal to i in the direction of j

x_i = Generalized position coordinate

ρ = Material density

u_i = Generalized displacement

Substituting the stress in terms of strain and temperature change with expression (A3.2):

(7.15) $$\frac{\partial \sigma_{ij}}{\partial x_i} = \sum_k \sum_l C_{ijkl} \frac{\partial \varepsilon_{kl}}{\partial x_i} - \frac{\alpha}{(1-2\nu)} \delta_{ij} \frac{\partial \Delta T}{\partial x_i}$$

C_{ijkl} is used to here to represent the stiffness matrix, not the heat capacity.

Using the definition of strain in terms of displacement: $\varepsilon_{ij} = \frac{1}{2}\left(\frac{\partial u_i}{\partial x_j} + \frac{\partial u_j}{\partial x_i} \right)$

Equation 7.15 becomes:

(7.16) $$\rho \frac{\partial^2 \vec{u}}{\partial t^2} - \mu \nabla^2 \vec{u} - (\lambda + \mu) \vec{\nabla} (\vec{\nabla} \square \vec{u}) + \frac{\alpha E}{(1-2\nu)} \vec{\nabla} T = 0$$

The thermal dynamics are derived from energy conservation. The loss of energy from a piece of material is equal to the integral of the emittance over a closed surface that bounds the piece of material:

$$(7.17)\quad \frac{dE}{dt} = -\int_{area} \vec{\xi} \cdot d\vec{A}$$

E = Energy

$\vec{\xi}$ = Emittance [energy / (sec * area)]

The surface integral is transformed into a volume integral:

$$(7.18)\quad \frac{dE}{dt} = -\int_{area} \vec{\xi} \cdot d\vec{A} \rightarrow -\int_{volume} (\nabla \cdot \vec{\xi}) dV$$

If the change in energy is only attributed to heat flow, the left hand side of 7.18 becomes:

$$(7.19)\quad \frac{dE}{dt} = \frac{dQ}{dt} = T\frac{dS}{dt}$$

The energy emittance is related to temperature through the Boltzmann transport equation. Under the relaxation time approximation and in quasi-equilibrium it can be shown that:

$$(7.20)\quad \vec{\xi} = -\kappa(\nabla T)$$

κ = Thermal conductivity

Substituting 7.20 into 7.18 yields:

$$(7.21)\quad \frac{dE}{dt} = \int_{volume} \kappa \nabla^2 T dV$$

Rewriting the energy in terms of entropy:

$$(7.22)\quad T\frac{dS}{dt} = \int_{volume} \kappa \nabla^2 T dV$$

This may be rewritten in terms of entropy per unit volume:

$$(7.23)\quad T\frac{ds}{dt} = \kappa \nabla^2 T$$

When the constitutive equation for entropy is substituted into 7.23 the usual Fourier Law is obtained:

$$(7.24)\quad c\rho\frac{\partial T}{\partial t} = \kappa \nabla^2 T - \frac{E\alpha T_{init}}{(1-2\nu)}\left[\frac{\partial}{\partial t}(\varepsilon_{11}+\varepsilon_{22}+\varepsilon_{33})\right]$$

ν = Poisson's ratio

Equation 7.24 may be written in terms of displacement:

$$(7.25)\quad \kappa \nabla^2 T - c\rho\frac{\partial T}{\partial t} - \frac{\alpha E T_{init}}{(1-2\nu)}\vec{\nabla}\cdot\frac{\partial \vec{u}}{\partial t} = 0$$

Equations 7.16 and 7.25 are the coupled thermo-elastic equations that will be used to build the finite element model.

Chapter 8

Finite element modeling

8.1 Bulk Behavior

Finite element analysis enables solutions for systems of partial differential equations to be generated for boundary problems over complicated geometries. A bounded, solid geometry is represented by a set of nodes occupying the same space whose individual displacements are governed by the sum of the forces at each node. The forces and displacements need not describe actual motion; they may describe a scalar field such as temperature and the forces may be gradients in concentration of some quantity. The generalized forces may be generated external to the geometry, such as a gradient in electrical potential, or they may be imposed by neighboring nodes. A system of matrices is created to describe the loads, displacements, and reaction forces related by a stiffness matrix:

{reaction matrix}+{load matrix}={stiffness matrix}{displacement matrix}

A general approach to finding a solution (determining the displacements) is to supply initial conditions, invert the stiffness matrix, and solve for the displacement matrix. This method may be used to iterate to static solutions, or study systems that evolve in time.

FEMLAB is a general-purpose partial differential equation solver capable of finding solutions to complex eigenvalue problems. This chapter outlines the creation of a three-dimensional finite element model to determine the quality factor of resonant silicon structures. The relevant governing physical equations are presented, along with the necessary boundary conditions to solve for a set of eigenvalues that represent the complex resonant frequency spectrum of the device. The quality factor is determined indirectly through the ratio of the real and imaginary parts of the eigenvalue, as shown in Appendix 1.

The displacements to be solved for in this model are the positions, velocities, and temperatures of all the nodes. Since the model is three dimensional, each node therefore has seven degrees of freedom (three displacement, three velocity, and one temperature). It is assumed that these quantities are all separable with respect to time and space, and all oscillate with the same complex frequency. Since it is known that the temperature field is in general not in phase with the displacements of the nodes, the displacements, velocities, and temperatures are themselves complex quantities to account for the phase difference.

The partial differential equations that describe the anelastic behavior of the oscillating structure are in essence an elastic equation derived from balancing forces, and a heat diffusion equation with a source term. The coupled equations of thermoelasticity as derived in Chapter 7 for an isotropic material:

$$\rho\frac{\partial^2\vec{u}}{\partial t^2}-\mu\nabla^2\vec{u}-(\lambda+\mu)\vec{\nabla}(\vec{\nabla}\cdot\vec{u})+\frac{\alpha E}{(1-2\nu)}\vec{\nabla}T=0 \tag{8.1}$$

$$\kappa\nabla^2T-c\rho\frac{\partial T}{\partial t}-\frac{\alpha ET_{init}}{(1-2\nu)}\vec{\nabla}\cdot\frac{\partial\vec{u}}{\partial t}=0 \tag{8.2}$$

ρ = Material density

$\vec{u}=\vec{u}(x,y,z,t)$ = (Complex) displacement as a function of position and time

μ = Lamé coefficient - $\mu=\dfrac{E}{2(1+\nu)}$

λ = Lamé coefficient - $\lambda=\dfrac{E}{1+\nu}\left(\dfrac{\nu}{1-2\nu}\right)$

α = Coefficient of thermal expansion

E = Young's modulus

ν = Poisson's ratio

$T=T(x,y,z,t)$ = (Complex) Temperature as a function of position and time

κ = Thermal conductivity

c = Specific heat capacity

T_{init} = Initial (uniform) temperature of material

To somewhat simplify equation 8.1 and 8.2 the following substitution is made:

(8.3) $$\beta = \frac{-\alpha E}{(1-2\nu)}$$

The equations become:

(8.4) $$\rho\frac{\partial^2\vec{u}}{\partial t^2} - \mu\nabla^2\vec{u} - (\lambda+\mu)\vec{\nabla}(\vec{\nabla}\cdot\vec{u}) - \beta\vec{\nabla}T = 0$$

(8.5) $$\kappa\nabla^2 T - c\rho\frac{\partial T}{\partial t} + \beta T_{init}\vec{\nabla}\cdot\frac{\partial\vec{u}}{\partial t} = 0$$

Vector equation (8.3) is then broken into three scalar equations:

(8.6) $\vec{u} = u_x\hat{i} + u_y\hat{j} + u_z\hat{k}$

$u_i = u_i(x, y, z, t) =$ Displacement in the i direction as a function of position and time

(8.7a) $$-\hat{i}\mu(\frac{\partial^2 u_x}{\partial x^2}+\frac{\partial^2 u_x}{\partial y^2}+\frac{\partial^2 u_x}{\partial z^2}) - (\lambda+\mu)(\hat{i}\frac{\partial^2 u_x}{\partial x^2}+\hat{i}\frac{\partial^2 u_y}{\partial x\partial y}+\hat{i}\frac{\partial^2 u_z}{\partial x\partial z}) - \beta(\hat{i}\frac{\partial T}{\partial x}) = -\hat{i}\rho\frac{\partial^2 u_x}{\partial t^2}$$

(8.7b) $$-\hat{j}\mu(\frac{\partial^2 u_y}{\partial x^2}+\frac{\partial^2 u_y}{\partial y^2}+\frac{\partial^2 u_y}{\partial z^2}) - (\lambda+\mu)(\hat{j}\frac{\partial^2 u_x}{\partial y\partial x}+\hat{j}\frac{\partial^2 u_y}{\partial y^2}+\hat{j}\frac{\partial^2 u_z}{\partial y\partial z}) - \beta(\hat{j}\frac{\partial T}{\partial y}) = -\hat{j}\rho\frac{\partial^2 u_y}{\partial t^2}$$

(8.7c) $$-\hat{k}\mu(\frac{\partial^2 u_z}{\partial x^2}+\frac{\partial^2 u_z}{\partial y^2}+\frac{\partial^2 u_z}{\partial z^2}) - (\lambda+\mu)(\hat{k}\frac{\partial^2 u_x}{\partial z\partial x}+\hat{k}\frac{\partial^2 u_y}{\partial z\partial y}+\hat{k}\frac{\partial^2 u_z}{\partial z^2}) - \beta(\hat{k}\frac{\partial T}{\partial z}) = -\hat{k}\rho\frac{\partial^2 u_z}{\partial t^2}$$

(The time derivatives have been moved to the right hand side.)

The associated scalar equations are:

(8.8a) $$-\mu(\frac{\partial^2 u_x}{\partial x^2}+\frac{\partial^2 u_x}{\partial y^2}+\frac{\partial^2 u_x}{\partial z^2}) - (\lambda+\mu)(\frac{\partial^2 u_x}{\partial x^2}+\frac{\partial^2 u_y}{\partial x\partial y}+\frac{\partial^2 u_z}{\partial x\partial z}) - \beta(\frac{\partial T}{\partial x}) = -\rho\frac{\partial^2 u_x}{\partial t^2}$$

(8.8b) $$-\mu\left(\frac{\partial^2 u_y}{\partial x^2}+\frac{\partial^2 u_y}{\partial y^2}+\frac{\partial^2 u_y}{\partial z^2}\right)-(\lambda+\mu)\left(\frac{\partial^2 u_x}{\partial y \partial x}+\frac{\partial^2 u_y}{\partial y^2}+\frac{\partial^2 u_z}{\partial y \partial z}\right)-\beta\left(\frac{\partial T}{\partial y}\right)=-\rho\frac{\partial^2 u_y}{\partial t^2}$$

(8.8c) $$-\mu\left(\frac{\partial^2 u_z}{\partial x^2}+\frac{\partial^2 u_z}{\partial y^2}+\frac{\partial^2 u_z}{\partial z^2}\right)-(\lambda+\mu)\left(\frac{\partial^2 u_x}{\partial z \partial x}+\frac{\partial^2 u_y}{\partial z \partial y}+\frac{\partial^2 u_z}{\partial z^2}\right)-\beta\left(\frac{\partial T}{\partial z}\right)=-\rho\frac{\partial^2 u_z}{\partial t^2}$$

Heat equation (8.5) becomes:

(8.9) $$-\kappa\left(\frac{\partial^2 T}{\partial x^2}+\frac{\partial^2 T}{\partial y^2}+\frac{\partial^2 T}{\partial z^2}\right)-\beta T_{init}\left(\frac{\partial}{\partial x}\frac{\partial u_x}{\partial t}+\frac{\partial}{\partial y}\frac{\partial u_y}{\partial t}+\frac{\partial}{\partial z}\frac{\partial u_z}{\partial t}\right)=-c\rho\frac{\partial T}{\partial t}$$

(Only the time derivative of temperature is moved to the right hand side)

Next it is explicitly assumed that the temperature function and all displacement functions are separable in terms of position and time:

$u_i(x,y,z,t)=\hat{u}_i(x,y,z)f(t)$, $T(x,y,z,t)=\hat{T}(x,y,z)f(t)$

Where $f(t)=e^{(i\omega-\delta)t}=e^{\lambda t}$

The first order time derivatives of displacement and temperature are:

(8.10) $$\frac{\partial u_i}{\partial t}=\hat{u}_i\frac{\partial f}{\partial t}=\lambda\hat{u}_i f(t)=\lambda u_i$$

(8.11) $$\frac{\partial T}{\partial t}=\hat{T}\frac{\partial f}{\partial t}=\lambda\hat{T}f(t)=\lambda T$$

The goal is develop a system of eigenvalue equations and solve for lambda. Using equation 2.3, the quality factor is determined to be: $Q=\dfrac{\mathrm{Im}\{\lambda\}}{-2\cdot\mathrm{Re}\{\lambda\}}$

Due to the fact that equations (8.8) and equation (8.9) contain different order time derivatives, the three elastic equations must be rewritten in terms of six first order time derivative equations. Three more general displacements are introduced in the process. The second order time derivatives are rewritten in terms of the first order time derivative of a velocity:

$\frac{\partial^2 u_i}{\partial t^2} \rightarrow \frac{\partial \dot{u}_i}{\partial t} = \lambda \dot{u}_i$ where $\dot{u}_i = \frac{\partial u_i}{\partial t}$ is treated as a new independent variable.

The elastic equations become:

(8.12a) $\dot{u}_x = \lambda u_x$

(8.12b) $-\mu(\frac{\partial^2 u_x}{\partial x^2} + \frac{\partial^2 u_x}{\partial y^2} + \frac{\partial^2 u_x}{\partial z^2}) - (\lambda + \mu)(\frac{\partial^2 u_x}{\partial x^2} + \frac{\partial^2 u_y}{\partial x \partial y} + \frac{\partial^2 u_z}{\partial x \partial z}) - \beta(\frac{\partial T}{\partial x}) = -\rho \lambda \dot{u}_x$

(8.12c) $\dot{u}_y = \lambda u_y$

(8.12d) $-\mu(\frac{\partial^2 u_y}{\partial x^2} + \frac{\partial^2 u_y}{\partial y^2} + \frac{\partial^2 u_y}{\partial z^2}) - (\lambda + \mu)(\frac{\partial^2 u_x}{\partial y \partial x} + \frac{\partial^2 u_y}{\partial y^2} + \frac{\partial^2 u_z}{\partial y \partial z}) - \beta(\frac{\partial T}{\partial y}) = -\rho \lambda \dot{u}_y$

(8.12e) $\dot{u}_z = \lambda u_z$

(8.12f) $-\mu(\frac{\partial^2 u_z}{\partial x^2} + \frac{\partial^2 u_z}{\partial y^2} + \frac{\partial^2 u_z}{\partial z^2}) - (\lambda + \mu)(\frac{\partial^2 u_x}{\partial z \partial x} + \frac{\partial^2 u_y}{\partial z \partial y} + \frac{\partial^2 u_z}{\partial z^2}) - \beta(\frac{\partial T}{\partial z}) = -\rho \lambda \dot{u}_z$

The heat equation:

(8.13) $-k(\frac{\partial^2 T}{\partial x^2} + \frac{\partial^2 T}{\partial y^2} + \frac{\partial^2 T}{\partial z^2}) - \beta T_{init}(\frac{\partial}{\partial x}\dot{u}_x + \frac{\partial}{\partial y}\dot{u}_y + \frac{\partial}{\partial z}\dot{u}_z) = -c\rho\lambda T$

These are the seven equations needed for the FEMLAB model. While this should work in theory, due to the fact that the equations are weakly coupled, the model will not converge to meaningful solutions if entered this way.

To adjust the relative magnitudes of the equation terms, it is useful to revisit equations 8.4 and 8.5. The goal in rescaling the equations is to attempt to get all the terms to be closer in magnitude (and dimensionless). Assuming that the spatial derivatives are of the same magnitude, it is considerably simpler to rescale the equations if some of the spatial derivatives are disregarded for illustrative purposes. Equations 8.4 and 8.5 are written:

$$\frac{\partial^2 u}{\partial t^2} - \frac{\mu}{\rho}\frac{\partial^2 u}{\partial x^2} - \frac{\beta}{\rho}\frac{\partial T}{\partial x} = 0 \tag{8.14}$$

$$\frac{\partial^2 T}{\partial x^2} - \frac{c\rho}{\kappa}\frac{\partial T}{\partial t} + \frac{\beta T_{init}}{\kappa}\frac{\partial}{\partial x}\frac{\partial u}{\partial t} = 0 \tag{8.15}$$

Let $t = \frac{\tau}{\omega}$, $x = \frac{\varphi}{k}$, $u = u_o\tilde{u}$, $T = T_0\tilde{T}$

$\tau, \varphi, \tilde{u}, \tilde{T}$ are all dimensionless quantities, and ω, k, u_o, T_o are constants of the model that are to be determined.

Substitution of these newly defined variables into 8.14 and 8.15 yields the following:

$$u_0\omega^2\frac{\partial^2\tilde{u}}{\partial\tau^2} - \frac{\mu u_0 k^2}{\rho}\frac{\partial^2\tilde{u}}{\partial\varphi^2} - \frac{\beta T_0 k}{\rho}\frac{\partial\tilde{T}}{\partial\varphi} = 0 \tag{8.16}$$

$$T_0k^2\frac{\partial^2\tilde{T}}{\partial\varphi^2} - \frac{c\rho T_0\omega}{\kappa}\frac{\partial\tilde{T}}{\partial\tau} + \frac{\beta T_{init}u_0\omega k}{\kappa}\frac{\partial}{\partial\varphi}\frac{\partial\tilde{u}}{\partial\tau} = 0 \tag{8.17}$$

First the terms on the left are simplified:

$$\frac{\partial^2\tilde{u}}{\partial\tau^2} - \frac{\mu k^2}{\rho\omega^2}\frac{\partial^2\tilde{u}}{\partial\varphi^2} - \frac{\beta T_0 k}{\rho u_0\omega^2}\frac{\partial\tilde{T}}{\partial\varphi} = 0 \tag{8.18}$$

$$\frac{\partial^2\tilde{T}}{\partial\varphi^2} - \frac{c\rho\omega}{\kappa k^2}\frac{\partial\tilde{T}}{\partial\tau} + \frac{\beta T_{init}u_0\omega}{\kappa T_0 k}\frac{\partial}{\partial\varphi}\frac{\partial\tilde{u}}{\partial\tau} = 0 \tag{8.19}$$

In equation 8.18, the second term will be of the order one if $\omega^2 = k^2 \frac{\mu}{\rho}$. This defines the usual dispersion relation of the acoustic wave. In equation 10.19, the second term will be of the order one if $\omega = k^2 \frac{\kappa}{c\rho}$. This defines the usual dispersion relation for the thermal diffusion equation. To satisfy both constraints, specific length and time scales can be identified: $k = \frac{c}{\kappa}\sqrt{\rho\mu}$ and $\omega = \frac{c\mu}{\kappa}$.

Equations 8.14 and 8.15 are now written as:

(8.20) $$\frac{\partial^2 \tilde{u}}{\partial \tau^2} - \frac{\partial^2 \tilde{u}}{\partial \varphi^2} - \frac{\beta T_0 k}{\rho u_0 \omega^2}\frac{\partial \tilde{T}}{\partial \varphi} = 0$$

(8.21) $$\frac{\partial^2 \tilde{T}}{\partial \varphi^2} - \frac{\partial \tilde{T}}{\partial \tau} + \frac{\beta T_{init} u_0 \omega}{\kappa T_0 k}\frac{\partial}{\partial \varphi}\frac{\partial \tilde{u}}{\partial \tau} = 0$$

We can also specify T_0 and u_0. It is not possible (in general) to define these quantities such that $\frac{\beta T_0 k}{\rho u_0 \omega^2} = 1$ and $\frac{\beta T_{init} u_0 \omega}{\kappa T_0 k} = 1$. However the two terms may be rewritten in terms of the ratio of T_0 and u_0. This ratio may be chosen such that the cross coupling terms are equal to each other. Substituting for ω and k and isolating the ratio of T_0 and u_0 the coupling terms are written:

$$\frac{\beta T_0 k}{\rho u_0 \omega^2} = \frac{\beta k}{\rho \omega^2}\left(\frac{T_0}{u_0}\right) = \frac{\beta \kappa}{c\mu\sqrt{\rho\mu}}\left(\frac{T_0}{u_0}\right) \text{ and } \frac{\beta T_{init} u_0 \omega}{\kappa T_0 k} = \frac{\beta T_{init}\omega}{\kappa k}\left(\frac{u_0}{T_0}\right) = \frac{\beta T_{init}\sqrt{\mu}}{\kappa\sqrt{\rho}}\left(\frac{u_0}{T_0}\right)$$

If the coupling terms are set equal to one another, an expression is found for the ratio of u_0 and T_0:

$$\frac{u_o}{T_o} = \frac{\kappa}{\mu\sqrt{cT_{init}}}$$

Equations 8.14 and 8.15 are now written as:

(8.22) $$\frac{\partial^2 \tilde{u}}{\partial \tau^2} - \frac{\partial^2 \tilde{u}}{\partial \varphi^2} - \beta\sqrt{\frac{T_{init}}{c\rho\mu}}\frac{\partial \tilde{T}}{\partial \varphi} = 0$$

(8.23) $$\frac{\partial^2 \tilde{T}}{\partial \varphi^2} - \frac{\partial \tilde{T}}{\partial \tau} + \beta\sqrt{\frac{T_{init}}{c\rho\mu}}\frac{\partial}{\partial \varphi}\frac{\partial \tilde{u}}{\partial \tau} = 0$$

(8.24) Let $$\Xi = \beta\sqrt{\frac{T_{init}}{c\rho\mu}}$$

The final rescaled form of 8.14 and 8.15 are now:

(8.25) $$\frac{\partial^2 \tilde{u}}{\partial \tau^2} - \frac{\partial^2 \tilde{u}}{\partial \varphi^2} - \Xi\frac{\partial \tilde{T}}{\partial \varphi} = 0$$

(8.26) $$\frac{\partial^2 \tilde{T}}{\partial \varphi^2} - \frac{\partial \tilde{T}}{\partial \tau} + \Xi\frac{\partial}{\partial \varphi}\frac{\partial \tilde{u}}{\partial \tau} = 0$$

In summary, the scales chosen are:

- Length: $x = \frac{\varphi}{k}$, $k = \frac{c}{\kappa}\sqrt{\rho\mu}$
- Time: $t = \frac{\tau}{\omega}$, $\omega = \frac{c\mu}{\kappa}$
- Displacement: $u = u_o\tilde{u}$
- Temperature: $T = T_0\tilde{T}$
- Coupling: $\frac{u_o}{T_o} = \frac{\kappa}{\mu\sqrt{cT_{init}}}$
- $\Xi = \beta\sqrt{\frac{T_{init}}{c\rho\mu}}$

Using this same technique, we rescale equations (8.12) and equation (8.13):

The elastic equations become:

(8.27a) $$\dot{u}_{\varphi} = \lambda u_{\varphi}$$

(8.27b) $$-\left(\frac{\partial^2 u_{\phi}}{\partial \varphi^2}+\frac{\partial^2 u_{\phi}}{\partial \phi^2}+\frac{\partial^2 u_{\phi}}{\partial \psi^2}\right)-\frac{(\lambda+\mu)}{\mu}\left(\frac{\partial^2 u_{\varphi}}{\partial \varphi^2}+\frac{\partial^2 u_{\phi}}{\partial \varphi \partial \phi}+\frac{\partial^2 u_{\psi}}{\partial \varphi \partial \psi}\right)-\Xi\left(\frac{\partial \tilde{T}}{\partial \varphi}\right)=-\lambda \dot{u}_{\varphi}$$

(8.27c) $$\dot{u}_{\phi} = \lambda u_{\phi}$$

(8.27d) $$-\left(\frac{\partial^2 u_{\phi}}{\partial \varphi^2}+\frac{\partial^2 u_{\phi}}{\partial \phi^2}+\frac{\partial^2 u_{\phi}}{\partial \psi^2}\right)-\frac{(\lambda+\mu)}{\mu}\left(\frac{\partial^2 u_{\varphi}}{\partial \phi \partial \varphi}+\frac{\partial^2 u_{\phi}}{\partial \phi^2}+\frac{\partial^2 u_{\psi}}{\partial \phi \partial \psi}\right)-\Xi\left(\frac{\partial \tilde{T}}{\partial \phi}\right)=-\lambda \dot{u}_{\phi}$$

(8.27e) $$\dot{u}_{\psi} = \lambda u_{\psi}$$

(8.27f) $$-\left(\frac{\partial^2 u_{\psi}}{\partial \varphi^2}+\frac{\partial^2 u_{\psi}}{\partial \phi^2}+\frac{\partial^2 u_{\psi}}{\partial \psi^2}\right)-\frac{(\lambda+\mu)}{\mu}\left(\frac{\partial^2 u_{\varphi}}{\partial \psi \partial x}+\frac{\partial^2 u_{\phi}}{\partial \psi \partial \phi}+\frac{\partial^2 u_{\psi}}{\partial \psi^2}\right)-\Xi\left(\frac{\partial \tilde{T}}{\partial \psi}\right)=-\lambda \dot{u}_{\psi}$$

The heat equation:

(8.28) $$-\left(\frac{\partial^2 \tilde{T}}{\partial \varphi^2}+\frac{\partial^2 \tilde{T}}{\partial \phi^2}+\frac{\partial^2 \tilde{T}}{\partial \psi^2}\right)-\Xi\left(\frac{\partial \dot{u}_{\lambda}}{\partial \varphi}+\frac{\partial \dot{u}_{\phi}}{\partial \phi}+\frac{\partial \dot{u}_{\psi}}{\partial \psi}\right)=-\lambda \tilde{T}$$

Here ϕ, φ, and ψ are the new rescaled spatial coordinates.

The rescaled thermoelastic equations now need to be entered in to the FAMLAB package. The general form that the FEMLAB eigenvalue solver is the following:

(8.29) $$-\nabla \cdot (c\nabla u + \alpha u - \gamma) + a \cdot u + \beta \cdot \nabla u = d_a \cdot \lambda \cdot u$$

$c, \alpha, \gamma, a, \beta, d_a$ are all matrices of coefficients. λ is the eigenvalue to be solved for, and u is the displacement matrix, which contains the eigenvectors that describe the displacement, velocity and temperature of each node in the model geometry:

$$u = \begin{bmatrix} \dot{u}_{\varphi} & u_{\varphi} & \dot{u}_{\phi} & u_{\phi} & \dot{u}_{\psi} & u_{\psi} & T \end{bmatrix}^T$$

Equations 8.27 and 8.28 are translated into FEMLAB with the following matrices (in the same order that they appear above):

The c matrix is a 7x7 matrix of 3x3 matrices:

$$c = \begin{bmatrix} c_{11} & c_{12} & c_{13} & c_{14} & c_{15} & c_{16} & c_{17} \\ c_{21} & c_{22} & c_{23} & c_{24} & c_{25} & c_{26} & c_{27} \\ c_{31} & c_{32} & c_{33} & c_{34} & c_{35} & c_{36} & c_{37} \\ c_{41} & c_{42} & c_{43} & c_{44} & c_{45} & c_{46} & c_{47} \\ c_{51} & c_{52} & c_{53} & c_{54} & c_{55} & c_{56} & c_{57} \\ c_{61} & c_{62} & c_{63} & c_{64} & c_{65} & c_{66} & c_{67} \\ c_{71} & c_{72} & c_{73} & c_{74} & c_{75} & c_{76} & c_{77} \end{bmatrix}$$

Where:

$$c_{21} = \begin{bmatrix} 2+\lambda/\mu & 0 & 0 \\ 0 & 1 & 0 \\ 0 & 0 & 1 \end{bmatrix}, c_{23} = \begin{bmatrix} 0 & \lambda/\mu & 0 \\ 1 & 0 & 0 \\ 0 & 0 & 0 \end{bmatrix}, c_{25} = \begin{bmatrix} 0 & 0 & \lambda/\mu \\ 0 & 0 & 0 \\ 1 & 0 & 0 \end{bmatrix}$$

$$c_{41} = \begin{bmatrix} 0 & 1 & 0 \\ \lambda/\mu & 0 & 0 \\ 0 & 0 & 0 \end{bmatrix}, c_{43} = \begin{bmatrix} 1 & 0 & 0 \\ 0 & 2+\lambda/\mu & 0 \\ 0 & 0 & 1 \end{bmatrix}, c_{45} = \begin{bmatrix} 0 & 0 & 0 \\ 0 & 0 & \lambda/\mu \\ 0 & 1 & 0 \end{bmatrix}$$

$$c_{61} = \begin{bmatrix} 0 & 0 & 1 \\ 0 & 0 & 0 \\ \lambda/\mu & 0 & 0 \end{bmatrix}, c_{63} = \begin{bmatrix} 0 & 0 & 0 \\ 0 & 0 & 1 \\ 0 & \lambda/\mu & 0 \end{bmatrix}, c_{65} = \begin{bmatrix} 1 & 0 & 0 \\ 0 & 1 & 0 \\ 0 & 0 & 2+\lambda/\mu \end{bmatrix}$$

$$c_{77} = \begin{bmatrix} 1 & 0 & 0 \\ 0 & 1 & 0 \\ 0 & 0 & 1 \end{bmatrix}$$

All other c submatrices are zero matrices.

The α matrix is a 7x7 matrix of 3x1 matrices. The non-zero matrices are:

$$\alpha_{27} = [\Xi \quad 0 \quad 0], \alpha_{47} = [0 \quad \Xi \quad 0], \alpha_{67} = [0 \quad 0 \quad \Xi]$$

The γ matrix is a 7x1 matrix of 3x1 matrices. There are no non-zero elements in this model.

The a matrix is a 7x7 matrix of scalars:

$$a = \begin{bmatrix} 0 & 1 & 0 & 0 & 0 & 0 & 0 \\ 0 & 0 & 0 & 0 & 0 & 0 & 0 \\ 0 & 0 & 0 & 1 & 0 & 0 & 0 \\ 0 & 0 & 0 & 0 & 0 & 0 & 0 \\ 0 & 0 & 0 & 0 & 0 & 1 & 0 \\ 0 & 0 & 0 & 0 & 0 & 0 & 0 \\ 0 & 0 & 0 & 0 & 0 & 0 & 0 \end{bmatrix}$$

The β matrix is a 7x7 matrix of 3x1 matrices. The non-zero matrices are:

$$\alpha_{72} = [-\Xi \quad 0 \quad 0], \alpha_{74} = [0 \quad -\Xi \quad 0], \alpha_{76} = [0 \quad 0 \quad -\Xi]$$

The d_a matrix is a 7x7 matrix of scalars:

$$d_a = \begin{bmatrix} i & 0 & 0 & 0 & 0 & 0 & 0 \\ 0 & -i & 0 & 0 & 0 & 0 & 0 \\ 0 & 0 & i & 0 & 0 & 0 & 0 \\ 0 & 0 & 0 & -i & 0 & 0 & 0 \\ 0 & 0 & 0 & 0 & i & 0 & 0 \\ 0 & 0 & 0 & 0 & 0 & -i & 0 \\ 0 & 0 & 0 & 0 & 0 & 0 & -i \end{bmatrix}$$

The imaginary numbers appear in this matrix to swap the real and imaginary parts of the eigenvalues that are sought. Because the damping magnitude (real part of the complex eigenvalue) is much smaller than the resonant frequency (imaginary part of the complex frequency) for the lightly damped oscillators in this study, the two are swapped so that FEMLAB may be able to find the eigenvalues more easily. (This is a subtlety of the program- it searches the real axis, not the imaginary axis, for solutions to the equations.)

8.2 Boundary Conditions

In these models, there are three types of boundaries that can be used. These are conditions on the equations that are applied at surfaces of the geometry under study. The surfaces may be anchored, meaning that there are no displacements at that surface; they may be free, meaning that there are no normal forces to the surface; certain models may also employ a symmetry boundary to reduce the model size and computation time. Creating mirror symmetry in the model is accomplished by choosing a plane where no displacement is allowed perpendicular to the plane, while motion is unconstrained in the plane itself. All of these boundary conditions include a zero heat flow condition, effectively insulating the model geometry. While this may be physically difficult to realize, it is assumed that the heat transfer to the environment is small, which greatly simplifies the analysis.

The boundaries are entered into FEMLAB in the general format:

$$n\cdot(c\nabla u+\alpha u-\gamma)+q\cdot u=g-h^{T}\cdot u\,;h\cdot u=r \tag{8.30}$$

Where c,α,γ are the same matrices as in equation 8.29, and u is the matrix of generalized displacement eigenvectors, as before. n is a normal vector to the surface of the geometry.

In all the boundary conditions for this model, the q, r and g matrices are set to zero.

h is a 7x7 matrix of scalars. For a free surface, h is a zero matrix. For an anchored boundary:

$$h = \begin{vmatrix} 1 & 0 & 0 & 0 & 0 & 0 & 0 \\ 0 & 1 & 0 & 0 & 0 & 0 & 0 \\ 0 & 0 & 1 & 0 & 0 & 0 & 0 \\ 0 & 0 & 0 & 1 & 0 & 0 & 0 \\ 0 & 0 & 0 & 0 & 1 & 0 & 0 \\ 0 & 0 & 0 & 0 & 0 & 1 & 0 \\ 0 & 0 & 0 & 0 & 0 & 0 & 0 \end{vmatrix}$$

For the symmetry boundary condition for about a plane parallel to the y-z plane:

$$h = \begin{vmatrix} 1 & 0 & 0 & 0 & 0 & 0 & 0 \\ 0 & 1 & 0 & 0 & 0 & 0 & 0 \\ 0 & 0 & 0 & 0 & 0 & 0 & 0 \\ 0 & 0 & 0 & 0 & 0 & 0 & 0 \\ 0 & 0 & 0 & 0 & 0 & 0 & 0 \\ 0 & 0 & 0 & 0 & 0 & 0 & 0 \\ 0 & 0 & 0 & 0 & 0 & 0 & 0 \end{vmatrix}$$

One of the subtleties of this model lies in the enforcement of the zero-force free boundary condition. The forces on an element are determined in terms of the local strain, and the thermal strain generated by local heating must be included in addition to the elastic strain. The strain of the material is related to the first spatial derivative of the displacement. In the FEMLAB general equation 8.29, there are two places to calculate first order spatial derivatives of the displacement matrix through non-zero elements of the α and β matrices. The thermal contribution to the strain in the bulk can be calculated in either of these matrices. The difference between the two lies in the fact that the α matrix is included in the boundary conditions, while the β matrix is not. For thermal strain to be included in the stress-free boundary condition in addition to the elastic strain, the thermal strain must be calculated in the α matrix. Appendix 3 contains the constitutive stress strain relations used to determine the force free boundary condition.

8.3 Material Properties of Silicon

The finite element model developed in the preceding sections was built for a material that is elastically and thermally isotropic. Silicon however is not. Since our present study is focused on beams and cantilevers, where stress and strain are developed along the longitudinal axis of the beam, and temperature gradients exist perpendicular to the longitudinal axis, choosing the thermal and elastic constants of silicon along those axes is a good approximation to the anisotropic solution. Specifically, this finite element model attempts to simulate micromachined beams whose bounding planes are all {100} planes. A convenient coordinate system to use is three mutually perpendicular axes in the <100> directions of the material. (Because silicon displays cubic symmetry, the constants along the three mutually perpendicular directions are the same.) Therefore, this model uses material properties determined along the <100> directions of silicon and applies them as if the material were isotropic. The thermal/mechanical properties for the model (listed below) are from reference [14]. All values are taken at 300K, and no more than three significant digits were kept for these calculations. It is unlikely that some of these parameters would actually be this well known for one of our gyroscope materials. However three significant digits are retained for comparing the finite element model to the analytical equations).

Young's modulus = 130 GPa
Poisson's ratio = 0.280
Thermal conductivity = 156 [W / (m*K)]
Coefficient of thermal expansion: 2.62e-6 / K
Density: 2330 kg / m^3
Specific heat (at constant pressure) = 713 [J / (kg*K)]

It is apparent upon inspecting the matrices used for the FEMLAB model that two numbers are needed for this simulation at this point- the ratio of the Lamé coefficients

and the coupling coefficient Ξ, both determined by the material properties of the oscillator:

$$\Xi = \beta\sqrt{\frac{T_{init}}{c\rho\mu}} = \frac{-\alpha E}{(1-2\nu)}\sqrt{\frac{T_{init}2(1+\nu)}{c\rho E}} = -\alpha\sqrt{\frac{ET_{init}}{c\rho}}\frac{\sqrt{2(1+\nu)}}{(1-2\nu)} \approx -0.0462 \tag{8.31}$$

$$\frac{\lambda}{\mu} = \frac{\frac{E}{1+\nu}\left(\frac{\nu}{1-2\nu}\right)}{\frac{E}{2(1+\nu)}} = \frac{2\nu}{1-2\nu} \approx 1.27 \tag{8.32}$$

These are the values that are used in all the simulations of this study.

8.4 Finite Element Models

The models that were studied are all variations of a doubly clamped simple beam. First, a study of mesh density was performed to provide some insight as to the convergence of the calculations of quality factor, as well as what calculations may be performed in a reasonable amount of time on a desktop computer. Next, the beam was simulated in the lowest flexural mode for comparison to the analytical results of Zener and Roukes. This provided a validation of the model's utility for modeling thermoelastic damping. This same beam was then simulated in the second resonant flexural mode to determine the impact on the quality factor.

Two variations on the doubly clamped beam were simulated- the addition of anchors, and also the addition of anchors and fillets. These geometries were used to try to understand the effect of these approximations to support structures that exist in the actual device structure. The figures below show the geometries modeled. The shaded portions show the faces that are held immobile.

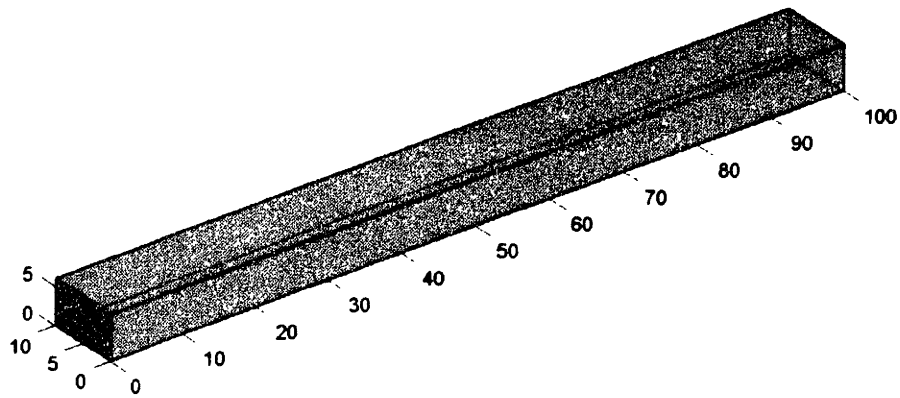

Figure 8.1: Simple beam

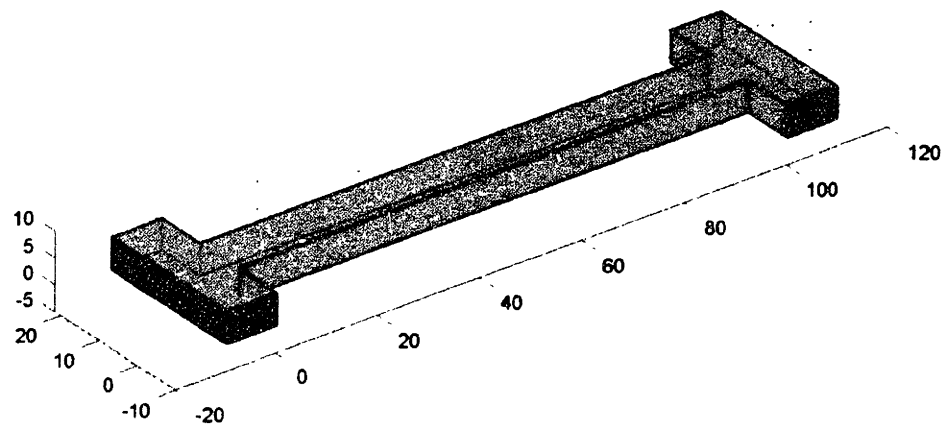

Figure 8.2: Beam with anchors

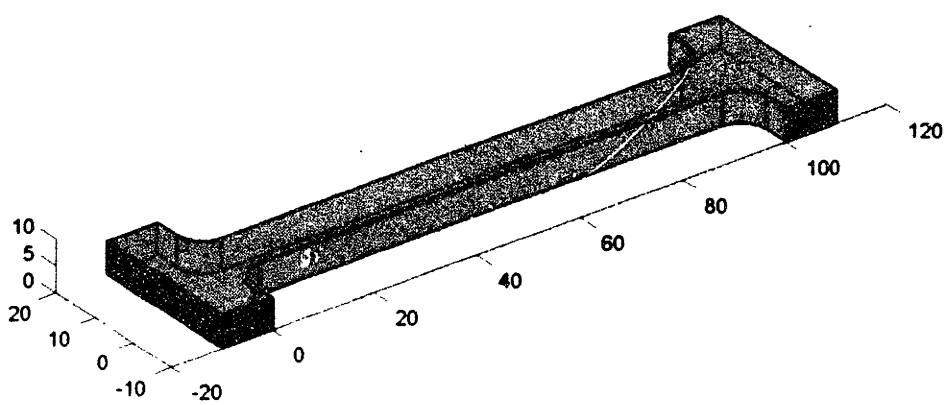

Figure 8.3: Beam with anchors and fillets

The basic beam dimensions (the beam dimensions without the anchors and fillets) used in these simulations were set at a constant ratio of five units wide, three units thick, and fifty units long. The ten to one ratio of length to width was chosen to compare the results of our studies to those of Roukes' paper, in which the quality factor for various sized beams (with the same length to width ratio) were calculated. In both these simulations and Roukes' calculations it is assumed that the beam vibrates in the direction of the width dimension. The width to height ratio was set to give the beam a similar number of mesh elements in both directions perpendicular to the longitudinal beam axis, but not more height than necessary, as it would add to the computational load.[8] Because the thermal gradients across the width of the beam are the cause of the damping behavior, it is necessary to have enough mesh elements across the width to capture this effect. Although no comparable gradients exist across the height of the beam during oscillation, the height of the beam contributes indirectly to the damping behavior through compression/tension of the material due to the Poisson ratio.[9] It is expected that a beam with a much greater relative height dimension would not exhibit as much strain in that dimension (due to plane strain conditions), and would therefore have a different quality factor.

The anchor dimensions used in the modeling were chosen through trial and error to include most of the stress and temperature distribution that extended into the anchor structure in order to capture the physical effects of their presence. The height of the anchor was chosen to be the same as that of the beam, each anchor extended two beam widths in the longitudinal direction of the beam axis, and each anchor extended past both sides of the beam a distance equal to one beam width. These models were run with three sides of each anchor held motionless (the three sides of the anchor rectangle not attached to the beam). In the simple beam model, the two end planes of the beam were held motionless.

Fillets were added to the geometry to smooth out the intersection between the beam and the anchors. Five models were run with the fillets, the radii of which were

---

[8] FEMLAB uses tetrahedral elements of roughly similar size to mesh three-dimensional geometries. Therefore the linear density of elements is not adjustable along the different beam dimensions.

[9] This effect is actually what complicated attempts at producing a two dimensional thermoelastic model in order to reduce the computational load.

added in increments of 10% of the beam width. These models were constrained to movement at the anchor faces in the same way as the anchor model with no fillets.

Due to the rescaling of the thermoelastic equations used in the FEMLAB model, the dimensions and resonant frequencies of a modeled oscillator must be rescaled to match actual dimensions. This is done using the equations from the rescaled equations:

$$\tau = \omega t\,, \quad \phi = kx$$

These equations are used to compare this finite element model to the analytical results of Zener and Roukes presented in Chapter 7. Using the material parameters for silicon, the value of ω and k are calculated to be:

$$k = \frac{c}{\kappa}\sqrt{\rho\mu} \approx 4.97 \cdot 10^{7}\, m^{-1}, \quad \omega = \frac{c\mu}{\kappa} = 2.32 \cdot 10^{11}\, Hz$$

The value of k is used to scale the real size into model dimensions. The value of ω is used to scale the expected resonant frequency using equation 2.5. This allows FEMLAB to solve for the resonant mode of interest.

To reduce the computational requirements for the models, symmetry conditions were used in all models whose resonant frequency mode exhibited mirror symmetry about a plane coincident with the cross section of the middle of the beam. This was the case for all of the beam models except for the simple beam vibrating in the second resonant mode. The reduced geometry meshes used are shown below.

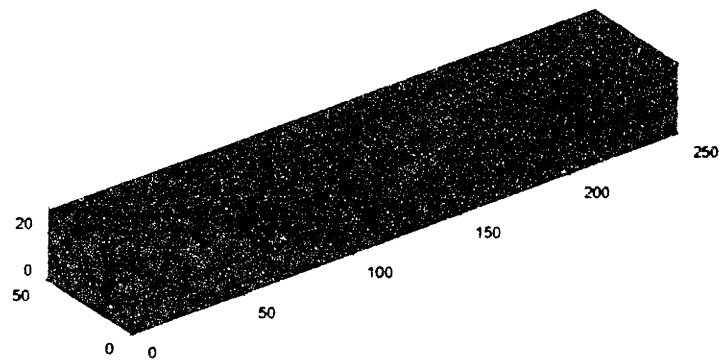

Figure 8.4: Half beam mesh

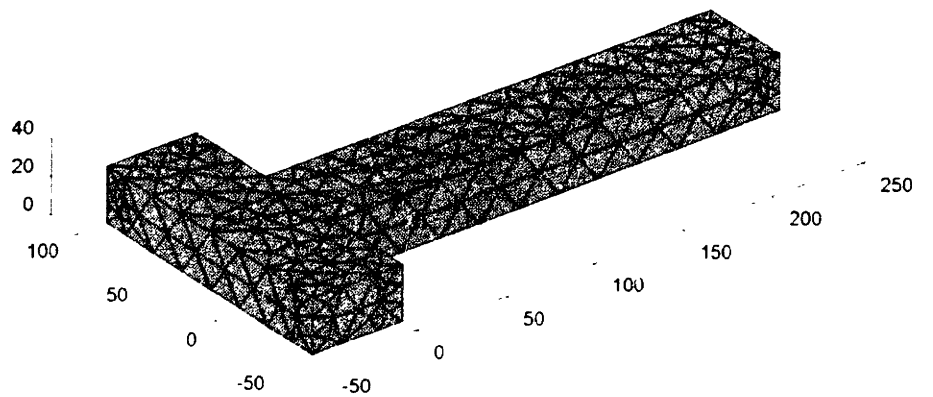

Figure 8.5: Half beam with anchor mesh

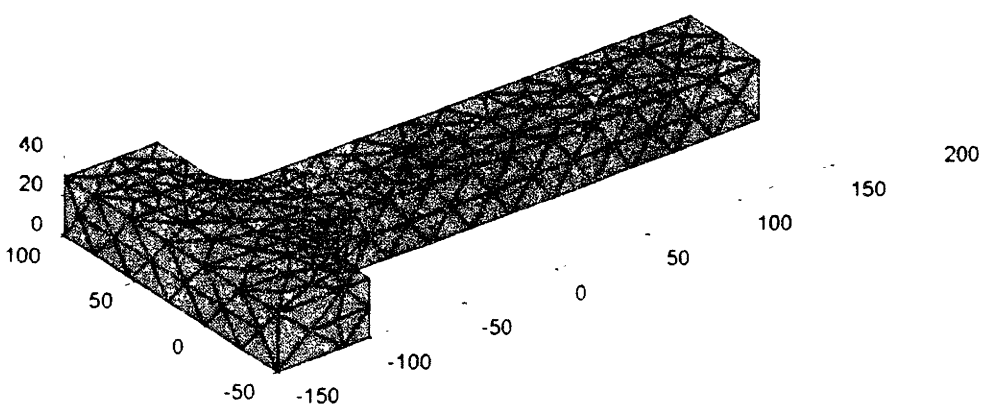

Figure 8.6: Half beam with anchors and fillets mesh – note the rounded edges near the intersection of the beam and the anchor

Chapter 9

Finite Element Analysis Results and Discussion

9.1 Model Validation

All of the simulations were performed on a desktop computer with a 2 GHz Intel® Pentium® 4 processor running Microsoft® Windows® 2000 with FEMLAB® version 2.2.

Using the thermoelastic FEMLAB model developed in Chapter 8, an initial study was conducted to determine how the number of mesh elements used in the beam model affects the calculated quality factor. It is expected that the simulation will become more accurate as the number of mesh elements increases, approaching the limit of a continuous model. Limited computational ability imposes the upper limit on the model accuracy: for all of these simulations the upper limit on the number of mesh elements was approximately fifteen hundred, with approximately five hundred associated nodes. Such a simulation requires one gigabyte of random access memory to run, although the simulation usually produces a result in only a few minutes.

The simple beam half-geometry was used to study the convergence of the calculated Q values. The scaled geometry was specifically chosen to represent the actual geometry of a device operating near peak damping ($\omega\tau = 1$). This was done for two reasons. First, the model experiences convergence problems if the 'device' is operating at a frequency that is too far from the damping peak. Good results are obtained for approximately three orders of magnitude in frequency on either side of the damping peak for this model[10]. For frequencies farther away, the simulation is able to identify the resonant frequency of operation, but the damping term becomes nonsensical due to numerical instability calculating the (change in the) temperature field. The second reason

[10] Results are obtainable farther away from the peak, but the model equations must be rescaled.

that the mesh study was performed near the peak damping frequency was to check the magnitude of the damping to make sure that it was approximately what the analytical model predicts for a maximum damping frequency. The expression for the minimum Q (corresponding to the maximum damping) is given by:

$$(9.1)\quad \frac{1}{Q_{ted}} = \frac{E\alpha^2 T_o}{C_\sigma}\frac{\omega\tau_z}{1+(\omega\tau_z)^2}$$

$$\omega\tau_z \to 1, \frac{1}{Q_{ted}} \to \frac{E\alpha^2 T_o}{2C_\sigma}$$

With the substitution of the values for silicon from Chapter 7, this expression gives a minimum Q value of approximately 12,400.

FEMLAB has a mesh feature that lets the user specify the mesh density in general terms. The options range from extremely coarse to extremely fine. Although the finer meshes were too fine to be able to run for this model, nine meshes of varying mesh element sizes were run. The average mesh element volume as a percentage of the total beam volume was recorded as well as the corresponding Q values; the results are shown in Figure 9.1.

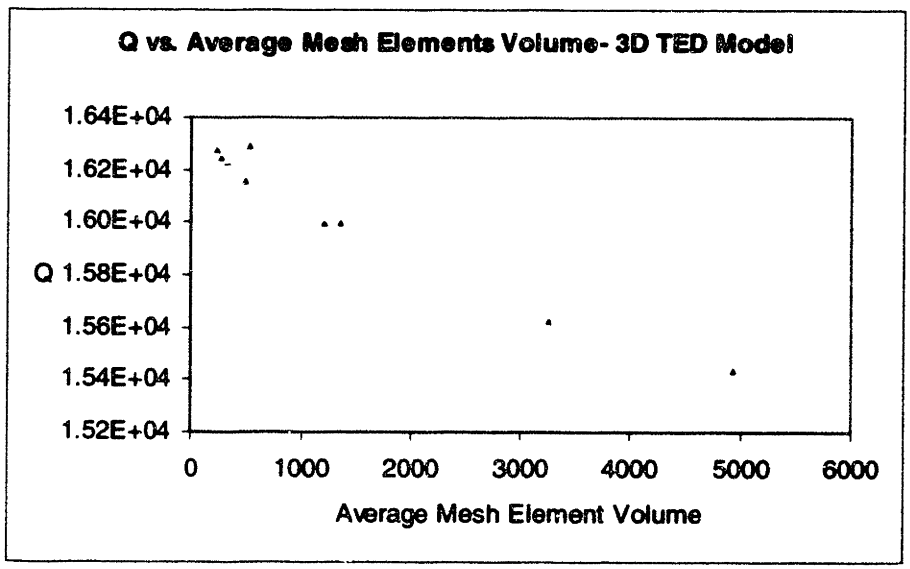

Figure 9.1: Calculated Q convergence with decreasing mesh element volume

This plot shows that as the average mesh element volume is decreased towards zero, Q increases and looks as if it will intersect the y-axis at a Q of approximately 16,400. The predicted Q value from equation 9.1 is 15,600. As the mesh density is increased, the calculated Q value drops and begins to level off. In the range of meshes studied, the higher quality factors that were calculated only varied by about 1%. As will be discussed, some difference is to be expected between the Q values of the finite element model and the analytical prediction of equation 9.1.

The beam size dimensions were then scaled up and down about the peak damping frequency. The length to width ratio is held fixed at 10. Thus, the fundamental mode frequency is *inversely* proportional to beam width in this experiment. The calculated quality factors from the finite element model were compared to those from the analytical expressions of Roukes and Zener (equations 9.23 and 9.24) for the same size beams. Figure 9.2 is a plot of calculated Q versus beam width; Figure 9.3 is a plot of the relative error in the finite element model in terms of Roukes' analytical expression for Q.[11]

[11] The beam widths in these figures scale down to nanometer dimensions- this is done only to compare the different calculations, not to imply this behavior would hold at that scale.

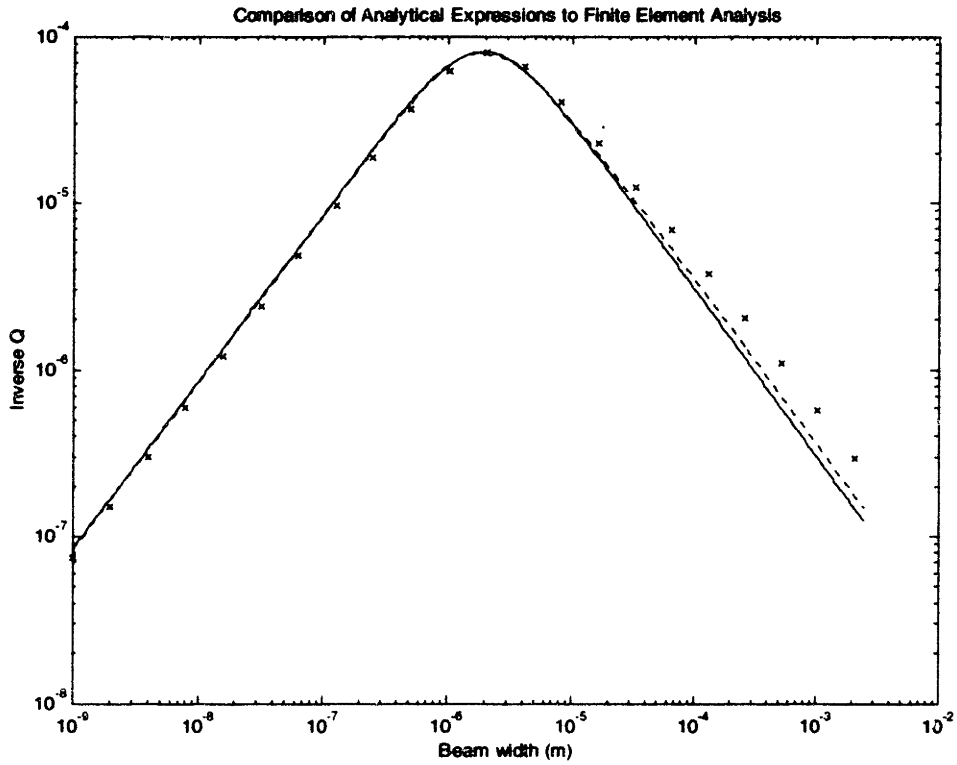

Figure 9.2: Comparison of finite element model and analytical expressions. The length to width ratio is held fixed to 10, so that scaling the beam width corresponds to scaling frequency. Since the frequency is proportional to width over length squared, the smaller widths in this figure have higher frequency fundamental modes. The solid line is Zener's calculation; the dashed line is Roukes formulation; the 'x' marks represent finite element results.

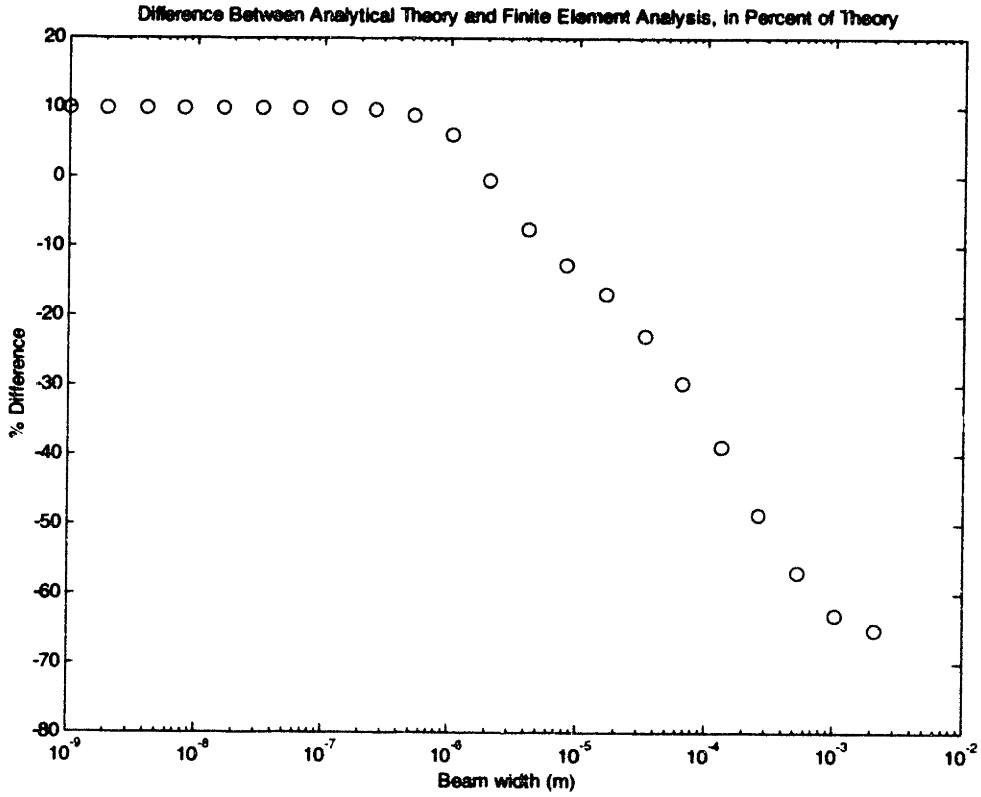

Figure 9.3: Difference (in % of analytical value) of finite element model and analytical expression of Roukes, for the same case studied in Figure2. The difference is calculated as $(Q_{roukes}-Q_{finite\ element})/ Q_{roukes}$

Qualitatively, Figure 9.2 shows that the finite element model is in reasonable agreement with the analytical expressions; it displays the same high frequency and low frequency dependence, as well as damping magnitude. Also, the finite element model deviates from the low frequency (large beam width) damping values predicted by Zener in the same manner as Roukes does. Both the finite element model and Roukes' analysis differ from Zener's through the inclusion of thermal gradients in the longitudinal direction in addition to the transverse thermal gradients, which become important at longer time scales. However, the calculations are not in quantitative agreement. It can be seen from Figure 9.3 that there is a constant 10% difference between the finite element calculation of quality factor and the calculation from Roukes' equation for thermoelastic Q at high frequencies (small beam widths). At low frequencies there is an increasingly

large discrepancy between the finite element and the analytical expression of Roukes. Various contributions to the discrepancy between the calculations may be thought as contributing to either the resonant frequency term or the damping term of the quality factor.

The finite element model predicts a different resonant frequency for a particular beam size than does Roukes' formula. This is easily verified by building a three-dimensional finite element elastic beam model (with no damping) and comparing the resonant frequency of the fundamental flexural mode to equation 2.5, which is used in the analytical expressions of quality factor. For the relative beam dimensions under study used, the difference in resonant frequencies is about 6%. FEMLAB predicts a value for the resonant frequency that is less than the analytical value. Since the quality factor is defined as $\frac{\omega_o}{2\delta}$, this deflates the quality factor predicted by the finite element model relative to the analytical expression for the same beam dimensions. If the constant 6% error were accounted for, it would shift the curve in Figure 9.3 up, increasing the relative error for small beam widths while decreasing it at large beam frequencies.

Although the contribution to the resonant frequency was determined to be off consistently by 6% relative to the analytical expressions for all frequencies, the relative error displayed in Figure 9.3 is seen to be frequency dependent. This behavior is attributed to the damping term of the quality factor. Figure 9.4 displays the calculated damping contributions from Zener's analytical expression as well as those from the finite element model. Figure 9.5 shows the relative error between the two calculations. It is interesting to note that both models agree qualitatively in that the damping becomes constant at high frequencies. This implies that the resonators always have the same decay envelope at high frequencies, independent of operating frequency.

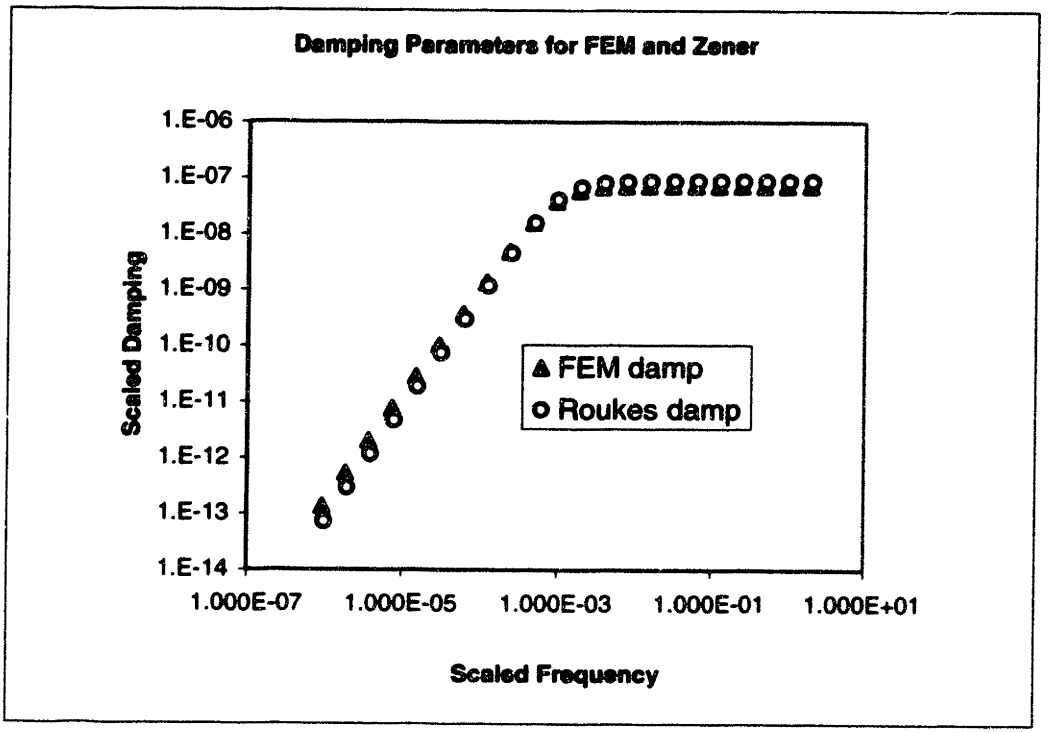

Figure 9.4: Damping parameters from analytical theory and the finite element model

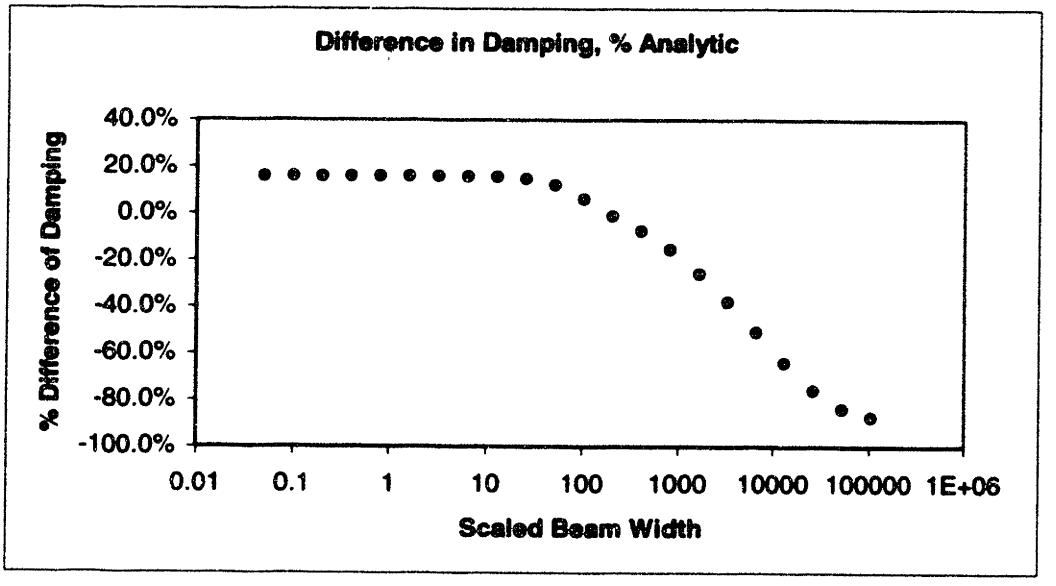

Figure 9.5: Difference (in % of theoretical value) of damping in the finite element model and Zener's analytical expression

The low frequency discrepancy between the calculations might be due in part to longitudinal currents that exist in the finite element model that are neglected in the derivation of the analytical expressions. Thermal gradients in the longitudinal direction exist over length scales over of a quarter of the beam length. This corresponds to an independent Debye peak at a lower frequency, since the characteristic thermal length scale is $\frac{length}{4}$ rather than $\frac{length}{10}$. Below the Debye peak studied here, the secondary peak may be apparent. This possibility should be investigated in further studies.

It is believed that most of the difference in the calculated quality factors is due to slightly different boundary conditions between the two models. In the finite element model, the material at the ends of the beam is held immobile- there can be no transverse strains with an applied load. In the analytical derivations, this condition is relaxed. The relaxed boundary conditions are more difficult to enforce in FEMLAB, which is why the different, slightly more realistic boundary conditions were enforced. This leads to different temperature distributions calculated from the two beam models, and ultimately different damping factors. Material near the end of the finite element beam is deformed more volume-wise than the material at the ends of the analytical model. This results in higher thermal gradients (and currents) existing at the ends of the finite element beam, causing increased damping. This effect may be offsetting other effects near the relaxation peak, explaining why the magnitude of damping is almost exactly in agreement with the analytical expressions of damping. If the material at the ends of the beam in the finite element model is allowed to relax in the height dimension, it is seen that at all frequencies the calculated quality factor increases between 8% and 20%. It is difficult to relax the material in the width dimension using FEMLAB, but it is believed that doing so would result in an even greater increase in the calculated quality factor.

At this point, the finite element model is determined to be a good indicator of the magnitude of thermoelastic damping for a simple structure. It is evident that more study is needed to determine (more quantitatively) the exact origin of the difference in calculated quality factors. However, due to the accurate qualitative behavior of the finite element model, calculations were carried out to determine the quality factor of beams

resonating in the second flexural mode, and several modifications to the beam were made in order to understand the impact of the geometrical changes.

9.2 Second Flexural Resonance Mode

The simple beam model was used to compare the quality factor of a beam vibrating in its second flexural mode to the quality factor of the same beam vibrating in the fundamental flexural mode. The same relative dimensions were used as in the model validation, a 5:50:3 width to length to height ratio for all the simulations. As shown in Figure 9.6, a similar Debye relaxation peak is produced for both modes. It is interesting that operating the same size device in the second flexural resonance mode has the effect of *either increasing or decreasing* the damping, depending on which side of the fundamental flexural Debye peak the device is operating. The key is the relationship between the operating frequency and the Debye peak frequency for a particular mode. If the damping peak cannot be shifted using different material parameters (the effect explored by the addition of germanium to the silicon lattice) or device geometry, the resonant mode may be chosen to optimize performance.

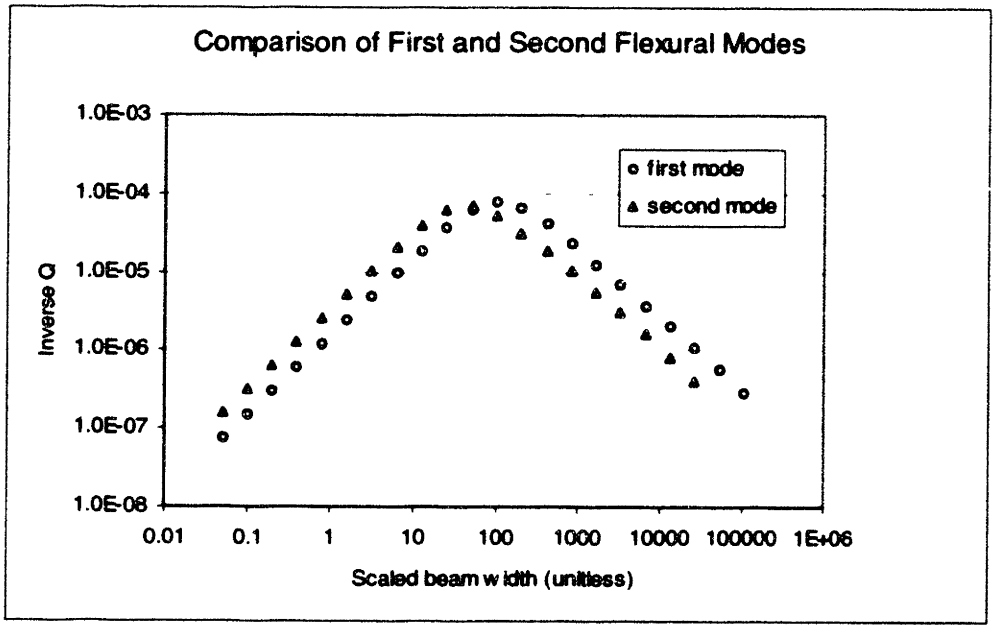

Figure 9.6: Comparison of the quality factor of beams in the first and second flexural mode

9.3 Beam with anchors

The simple beam is a crude approximation of a real beam structure, which cannot be isolated from its surroundings so completely. The addition of anchors to the ends of the beam allows the strain and temperature gradients to extend into the anchor material, somewhat diminishing the magnitude of the relative fields. A finite element model was run for the same beam geometry, with and without anchors to study the effect of the anchor supports. The geometry was chosen to coincide with the region of peak damping; the scaled width of the beams was fifty units. The results are shown in Table 9.1.

	Calculated Eigenvalue		
Model	**Real part (Damping)**	**Imaginary part (Resonant Freq.)**	**Q**
Beam no anchors	-6.01E-08	1.95E-03	16,300
Beam with anchors	-4.49E-08	1.74E-03	19,400

Table 9.1: Calculated eigenvalues of a beam with and without anchors

The addition of the anchors increases the quality factor of the beam by almost 20%. It is interesting to note that although the resonant frequency decreased with the addition of the anchors (due to an effective lengthening of the beam), the damping decreased (in magnitude) much more percentage-wise with the addition of the anchors, ultimately raising the quality factor. This reduction of strain near the anchor/beam boundary is seen to have a beneficial effect on the quality factor, confirming that relaxing the volumetric strain near the ends of the beam increases the performance of the resonator.

9.4 Beam with anchors and fillets

Fillets may be added to a resonator design to reduce strain at the anchor/beam interface. To study their effect on thermoelastic damping, fillets were added to the beam/anchor model and the quality factor was calculated for various sized fillets, given in Table 9.1 as a percentage of the beam width. The quality factor is seen to steadily decrease with the addition of larger fillets, which is the result of an increase in the

magnitude of the damping that outpaces the decrease in the resonant frequency. It is relatively simple to understand that the resonant frequency increases as the beam length effectively decreases. However, the damping behavior is a bit more complicated. As the effective beam width increases near the beam/anchor junction, the effective relaxation time for damping in that region increases, pushing this resonator system closer to the peak damping frequency. Since the relaxation time is proportional to the beam width squared, this effect scales rapidly with fillet radius. The balance of these effects is such that the increased damping outpaces the change in frequency, and the overall Q drops with larger fillets, for this geometry. At very low frequencies, the two effects would work together to raise the Q.

	Calculated Eigenvalue		
Fillet radius (% width)	Real part (Damping)	Imaginary part (Resonant Freq.)	Q
0	-4.49E-08	1.74E-03	19,400
10	-4.58E-08	1.76E-03	19,200
20	-4.78E-08	1.79E-03	18,700
30	-4.98E-08	1.83E-03	18,400
40	-5.20E-08	1.87E-03	18,000
50	-5.43E-08	1.91E-03	17,600

Table 9.2: Effect of fillets on quality factor

Chapter 10

Conclusions

10.1 Summary of Experimental Results

To improve the performance of gyroscopes manufactured at Draper Laboratory, the dependence of the quality factor (Q) upon gyroscope material was studied to identify material related damping issues. Quality factor measurements were performed on gyroscopes made from five different silicon-based materials- two containing no germanium and three with varying amounts of germanium. Gyroscopes made from the two materials that did not contain germanium had higher measured quality factors than the three wafer materials that contained 2%, 23%, and 30% germanium. The added germanium atoms are understood to reduce the local symmetry of the silicon structure and act as phonon scattering centers, reducing the thermal conductivity of the bulk material. It was shown that the thermal conductivity is a key parameter in thermoelastic damping, and this fact was use to explain our data. The results of the quality factor measurements are shown in Table 10.1.

	SiB epi	SiGeB 2%	SiGeB 23%	SiGeB 30%	B-diff
Devices Tested	9	9	9	10	10
Average frequency	12851	13327	10357	10785	12361
Average Q	177,000	62,800	27,100	23,400	219,000
Q standard deviation	10%	18%	6%	10%	20%

Table 10.1: Results of the quality factor measurements for gyroscopes made from five different wafer materials

10.2 Development of a Finite Element Model

The fact that thermoelastic damping is a performance limiting mechanism for Draper Laboratory's gyroscopes motivated the development of a finite element model to evaluate damping in simple resonant structures that are typical in MEMS design. The

finite element model displays the same qualitative predictive behavior as the analytical works of Zener and Roukes [1,2,3] for thermoelastic damping in a beam vibrating in a flexural mode. Figure 10.1 shows the amount of damping (here labeled as inverse Q) predicted by the finite element model in comparison to the analytical works of Zener and Roukes for thermoelastic damping in a beam of varying width. In this study, the length of the beam is fixed to be ten times the width.

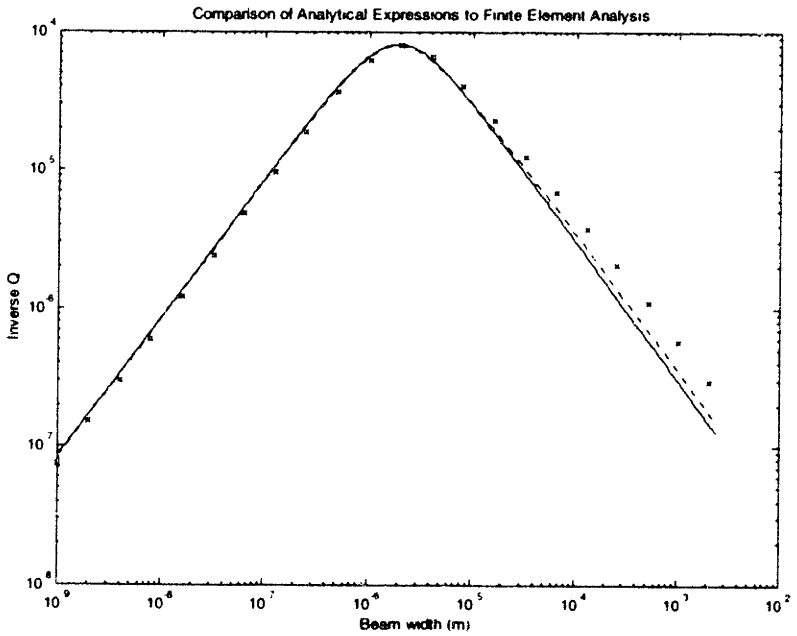

Figure 10.2: Comparison of finite element model and analytical expressions. The length to width ratio is held fixed to 10, so that scaling the beam width corresponds to scaling frequency. Since the frequency is proportional to width over length squared, the smaller widths in this figure have higher frequency fundamental modes.

The discrepancy between the Q factors calculated from the finite element model and the analytical equations is primarily caused by the slightly different boundary conditions between the different models. However, more investigation is needed to precisely determine the expected difference between the models. The model is therefore currently limited to order of magnitude damping calculations. Due to the fact that many different damping mechanisms may be competing during a particular device's operation, this model is still valuable in the respect that it produces an answer to the question, "Is this device design limited in performance by thermoelastic damping?" Also, because the

finite element model is in good qualitative agreement with theory, and is understood to be very sensitive to the boundary conditions, it underscores the fact that slight variations in device processing may be responsible for very different measured quality factors.

10.3 Implications for MEMS

Resonators with high quality factors are required in sensing applications to maintain low energy loss and high sensitivity. The finite element model developed in this thesis is useful for evaluating the magnitude of thermoelastic damping in geometries that are more complicated than those that can be described by existing analytical equations. This allows for an evaluation of the performance of a device before it is manufactured, potentially saving both development time and cost. This type of analysis lead to the following suggestions for improvement of Draper's gyroscopes: it is desirable to keep the germanium content low, the support beam width narrow, and the fillet size minimal to maintain a high quality factor.

The work contained in this thesis may be extended to other materials whose behavior is governed by multiphysics equations, such as thermoelectrics, ferroelectrics, and shape memory alloys. The finite element method is useful for evaluating the behavior of MEMS constructed from these materials, such as RF devices.

10.4 Future work

The finite element model developed in this thesis is an elastically and thermally isotropic model. This simplified the model development, but limited its scope of predictive power to simple structure elements where the stress is developed primarily along the <100> crystal direction in silicon. More complicated designs will require an anisotropic model for more accurate predictions of damping behavior.

Thermoelastic damping was identified as a leading source of damping in some our Draper Laboratory's gyroscopes, but other device designs may be found to be performance limited by other anelastic damping mechanisms. A suite of models could be

developed to predict other anelastic behavior such as damping due to point defect motion, dislocation motion, and grain boundary friction.

Appendix 1

Expressions for Quality Factor

In this appendix, several different equivalent expressions for Q are derived. These expressions are related to each other by the fractional amount of energy lost per cycle of oscillation. In addition to providing deeper insight, the equivalent formulas illustrate different ways to measure Q.

The definition of Q is the ratio of the total energy of the oscillator to the energy lost per radian of oscillation (it is assumed here that the system is highly underdamped, and that the total energy is approximately constant compared to the change in energy):

$$Q = \frac{E_{total}}{E_{lost\ per\ radian}}$$

From Chapter 2:

$$Q = \frac{\omega_o}{\Delta\omega}, \quad Q = \frac{\omega_o}{2\delta}$$

$\Delta\omega$ = Bandwidth at half the maximum amplitude

ω_o = Resonant frequency

δ = Damping parameter

The force balance expression for a one-dimensional oscillator with no damping is given by:

(A1.1) $m\ddot{x} + kx = 0$

$x = x(t)$ = Position as a function of time

m = Mass

k = Spring constant

The solution is $x(t) = x_o \cos(\omega t + \phi)$ where $\omega = \pm\sqrt{\frac{k}{m}}$

x_o = Amplitude of vibration

The phase angle and the plus/minus sign are dropped for simplicity:

(A1.2) $x(t) = x_o \cos(\omega t)$, $\omega = \omega_o = \sqrt{\frac{k}{m}}$

For an oscillator with damping, we add a term proportional to the velocity:

(A1.3) $m\ddot{x} + b\dot{x} + kx = 0$

b = Damping constant

It becomes easier to find a solution for the frequency in terms of the spring constant, damping constant and mass if we write the displacement test solution as complex number:

(A1.4) $x(t) = x_o \cos(\omega t) \rightarrow x(t) = x_o e^{i\omega t}$ (x_o is real)

Substituting back into (A1.3) and solving for the frequency:

(A1.5) $\omega = \frac{-ib \pm \sqrt{-b^2 + 4mk}}{-2m}$

For systems with small damping we make the approximation: $b^2 \ll 4mk$

Expression (A1.5) becomes:

(A1.6) $\omega = \frac{-ib \pm \sqrt{4mk}}{-2m} = i\frac{b}{2m} \pm \sqrt{\frac{k}{m}} \rightarrow i\delta \pm \omega_o$

Where $\delta = \frac{b}{2m}$

Substituting the frequency given by A1.6 back into expression A1.4 and taking the .eal part, it is verified that the expression of motion for a damped oscillator is:

(A1.7) $x(t) = x_o \cos(\omega_o t) \cdot e^{-\delta t}$

The quality factor for this system:

$$Q = \frac{E_{total}}{E_{lost\ per\ radian}}$$

The total energy is given by:

$$E_{total} = KE_{\max} = \frac{1}{2} m\omega^2 x_o^2$$

(Assume that this is almost constant over the cycle)

The energy lost is determined by the integral of the damping force over a distance moved in one radian of oscillation:

$$E_{lost\ per\ radian} = \int_{one\ radian} F_{damp}\,dx = \int_{one\ radian} b\frac{dx}{dt}\,dx = \int_0^{1/\omega} b\left(\frac{dx}{dt}\right)^2 dt$$

Substitute: $x = x_o \sin(\omega t)$, $\frac{dx}{dt} = x_o \omega \cos(\omega t)$

$$E_{lost} = b\omega^2 x_o^{\,2} \int_0^{1/\omega} \sin^2 \omega t dt = \frac{b\omega x_o^{\,2}}{2}$$

The end result:

$$\text{(A1.8)} \quad \frac{E_{total}}{E_{lost\ per\ radian}} = \frac{\frac{1}{2} m\omega^2 x_o^{\,2}}{\frac{1}{2} b\omega x_o^{\,2}} = \frac{m\omega}{b} = Q$$

If the system represented by (A1.3) includes a sinusoidal forcing function the expression becomes:

$$\text{(A1.9)} \quad m\ddot{x} + b\dot{x} + kx = F(t)$$

Here the forcing function is written as:

$$\text{(A1.10)} \quad F(t) = F_o e^{i\omega_d t} \quad (F_o \text{ is real})$$

ω_d = Drive frequency

The position may now be out of phase:

$$\text{(A1.11)} \quad x(t) = x_o e^{i(\omega_d t - \phi)}$$

Substituting (A1.10) and (A1.11) into (A1.9):

$$m\frac{d^2}{dt^2}(x_o e^{i(\omega_d t - \phi)}) + b\frac{d}{dt}(x_o e^{i(\omega_d t - \phi)}) + k(x_o e^{i(\omega_d t - \phi)}) = F_o e^{i\omega_d t}$$

Simplifying and relating the real and imaginary parts:

$$-mx_o\omega_d^2 + kx_o = F_o\cos\phi$$

$$\omega_d b x_o = F_o \sin\phi$$

The expressions may be combined with the trigonometric identity: $\sin^2\phi + \cos^2\phi = 1$

Solving for x_o:

$$x_o = \frac{F_o}{\left[\left(k - m\omega_d^2\right)^2 + \left(\omega_d b\right)^2\right]^{1/2}}$$

Rewriting in terms of the undamped resonant frequency and the damping parameter:

$$x_o = \frac{F_o}{m\left[\left(\omega_o^2 - \omega_d^2\right)^2 + 4\left(\omega_d\delta\right)^2\right]^{1/2}}$$

Figure A.1 shows a general plot of the amplitude versus driving frequency.

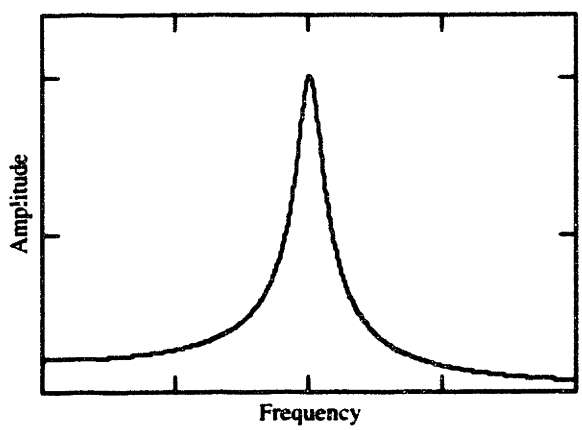

Figure A.1: Oscillator amplitude versus driving frequency

To find the resonant frequency of the damped system (the frequency at which maximum amplitude occurs), the derivative of this expression is taken with respect to the driving frequency, set equal to zero, and yields the following:

$$\omega_r = (\omega_o^2 - 2\delta^2)^{1/2}$$

The maximum value of amplitude is then given by:

$$x_{max} = \frac{F_o}{b\omega_d}$$

For weak damping, the expression for the amplitude close to the resonant frequency is:

$$x_o(\omega) = \frac{x_{max}\delta}{\left[(\omega_o - \omega)^2 + \delta^2\right]^{1/2}}$$

At $\omega = \omega_o \pm \delta$, $x_o = \frac{1}{2}x_{max}$ so that the half-maximum width of the resonance peak is twice delta: $\Delta\omega = 2\delta$, which is what makes the various expressions of the quality factor equivalent:

$$Q = \frac{E_{total}}{E_{lost\ per\ radian}} = \frac{\omega_o}{\Delta\omega} = \frac{\omega_o}{2\delta}$$

If a Q measurement is made of an oscillator where the displacement is proportional to a voltage output, the ratio of the voltages at maximum and half maximum displacement may be expressed in dB:

$$10\log\left(\frac{V_{max}}{V_{half\ max}}\right)dB = 10\log(2)dB = 3dB$$

Multiple Damping Terms

If there is more than one damping constant, due to different contributions to the damping, the force balance expression may be written as:

$$m\ddot{x} + (b_1 + b_2 + b_3 \ldots)\dot{x} + kx = m\ddot{x} + B\dot{x} + kx = 0$$

The quality factor may then be written as:

$$Q = \frac{m\omega_o}{B}$$

The total Q is then seen to add like parallel resistors in an electrical circuit:

$$\frac{1}{Q_{total}} = \frac{B}{m\omega_o} = \frac{(b_1 + b_2 + b_3 + \ldots)}{m\omega_o} = \frac{b_1}{m\omega_o} + \frac{b_2}{m\omega_o} + \frac{b_3}{m\omega_o} + \ldots = \frac{1}{Q_1} + \frac{1}{Q_2} + \frac{1}{Q_3} + \ldots$$

Appendix 2

Thermodynamic Relations

An unconstrained material with a positive coefficient of thermal expansion will expand upon heating, resulting in thermal strain. A fully constrained material will generate internal stresses to accommodate the thermal strain. In this manner it is evident that the mechanical properties of the solid (relating stress and strain) are coupled with the material's thermal properties. It is this coupling that also dictates that a material stressed adiabatically will experience a change in temperature, whose magnitude is determined by thermodynamic relations.

The first law of thermodynamics relates the energy of a system in terms of conjugate work variables. Although an expression may not be known for the total energy, energy differentials are easily describable, such as the differential of the free energy:

(A2.1) $dg = -sdT - \varepsilon d\sigma$

g = Gibb's free energy per unit volume

T = Temperature

s = Entropy per unit volume

This system contains two conjugate pairs: stress and strain, temperature and entropy. Any one of these variables can be related to any of the other two, such that an expression for temperature may be written as a function of stress and entropy. Therefore the differential change in temperature my be written as:

(A2.2) $$dT = \left(\frac{\partial T}{\partial \sigma}\right)_s d\sigma + \left(\frac{\partial T}{\partial s}\right)_\sigma ds$$

It is convenient to express temperature as a function of the stress and entropy because we are considering a system where no heat may be exchanged with the surroundings, such that the *ds* contribution to the differential is zero:

$$\text{(A2.3)}\quad ds = \frac{dQ}{T}, \qquad dQ = 0 \rightarrow ds = 0$$

Equation 7.3 reduces to:

$$\text{(A2.4)}\quad dT = \left(\frac{\partial T}{\partial \sigma}\right)_S d\sigma$$

To determine the value of $\left(\frac{\partial T}{\partial \sigma}\right)_S$, we substitute variables into an expression from differential calculus.
Using the relation:

$$\left(\frac{\partial x}{\partial y}\right)_z \left(\frac{\partial y}{\partial z}\right)_x \left(\frac{\partial z}{\partial x}\right)_y = -1$$

It may be written:

$$\text{(A2.5)}\quad \left(\frac{\partial T}{\partial \sigma}\right)_s \left(\frac{\partial \sigma}{\partial s}\right)_T \left(\frac{\partial s}{\partial T}\right)_\sigma = -1$$

The second term in A2.5 is determined by rewriting A2.1.

$$\text{(A2.6)}\quad dg = \left(\frac{\partial g}{\partial T}\right)_\sigma dT + \left(\frac{\partial g}{\partial \sigma}\right)_T d\sigma$$

Where it is understood that:

(A2.7) $$-\left(\frac{\partial g}{\partial T}\right)_{\sigma} = s\,, \quad -\left(\frac{\partial g}{\partial \sigma}\right)_{T} = \varepsilon$$

Noting the following two derivatives are equivalent:

(A2.8) $$\frac{\partial g}{\partial T \partial \sigma} = \frac{\partial g}{\partial \sigma \partial T}$$

The second term in A2.5 is determined to be the coefficient of thermal expansion.

(A2.9) $$\left(\frac{\partial s}{\partial \sigma}\right)_{T} = \left(\frac{\partial \varepsilon}{\partial T}\right)_{\sigma} = \alpha$$

The third derivative term in expression A2.5 is just the definition of heat capacity at constant stress:

(A2.10) $$\left(\frac{\partial s}{\partial T}\right)_{\sigma} = \frac{c_{\sigma}\rho}{T_{o}}$$

c_{σ} = Heat capacity at constant stress [energy / (volume * K)]

T_{o} = Initial temperature [K]

ρ = Density

Finally, the first term in A2.5 is found.

(A2.11) $$\left(\frac{\partial T}{\partial \sigma}\right)_{S} = -\frac{\left(\frac{\partial s}{\partial \sigma}\right)_{T}}{\left(\frac{\partial s}{\partial T}\right)_{\sigma}} = -\frac{\alpha T_{0}}{c_{\sigma}\rho}$$

Appendix 3

Stress-Strain Relations

The constitutive stress-strain equation for an isotropic material is:

(A3.1) $\varepsilon_{ij} = \sum_k \sum_l S_{ijkl}\sigma_{kl} + \alpha\Delta T\delta_{ij}$

ε = Strain vector

S_{ijkl} = Compliance matrix

σ = Stress vector

δ_{ij} = Kroenecker delta

Expanded in (simplified) matrix form:

$$\begin{bmatrix}\varepsilon_{11}\\ \varepsilon_{22}\\ \varepsilon_{33}\\ \gamma_{23}\\ \gamma_{31}\\ \gamma_{12}\end{bmatrix} = \frac{1}{E}\begin{bmatrix}1 & -\nu & -\nu & 0 & 0 & 0\\ -\nu & 1 & -\nu & 0 & 0 & 0\\ -\nu & -\nu & 1 & 0 & 0 & 0\\ 0 & 0 & 0 & 2(1+\nu) & 0 & 0\\ 0 & 0 & 0 & 0 & 2(1+\nu) & 0\\ 0 & 0 & 0 & 0 & 0 & 2(1+\nu)\end{bmatrix}\begin{bmatrix}\sigma_{11}\\ \sigma_{22}\\ \sigma_{33}\\ \tau_{23}\\ \tau_{31}\\ \tau_{12}\end{bmatrix} + \alpha\Delta T\begin{bmatrix}1\\1\\1\\0\\0\\0\end{bmatrix}$$

The stress state may be solved for:

(A3.2) $\sigma_{ij} = \sum_k \sum_l C_{ijkl}\varepsilon_{kl} - \frac{\alpha\Delta T}{(1-2\nu)}\delta_{ij}$

C_{ijkl} = Stiffness matrix

Expanded in matrix form:

$$\begin{bmatrix}\sigma_{11}\\ \sigma_{22}\\ \sigma_{33}\\ \tau_{23}\\ \tau_{31}\\ \tau_{12}\end{bmatrix} = E\begin{bmatrix}\frac{(1-\nu)}{(1+\nu)(1-2\nu)} & \frac{\nu}{(1+\nu)(1-2\nu)} & \frac{\nu}{(1+\nu)(1-2\nu)} & 0 & 0 & 0\\ \frac{\nu}{(1+\nu)(1-2\nu)} & \frac{(1-\nu)}{(1+\nu)(1-2\nu)} & \frac{\nu}{(1+\nu)(1-2\nu)} & 0 & 0 & 0\\ \frac{\nu}{(1+\nu)(1-2\nu)} & \frac{\nu}{(1+\nu)(1-2\nu)} & \frac{(1-\nu)}{(1+\nu)(1-2\nu)} & 0 & 0 & 0\\ 0 & 0 & 0 & \frac{1}{2(1+\nu)} & 0 & 0\\ 0 & 0 & 0 & 0 & \frac{1}{2(1+\nu)} & 0\\ 0 & 0 & 0 & 0 & 0 & \frac{1}{2(1+\nu)}\end{bmatrix}\begin{bmatrix}\varepsilon_{11}\\ \varepsilon_{22}\\ \varepsilon_{33}\\ \gamma_{23}\\ \gamma_{31}\\ \gamma_{12}\end{bmatrix} - \frac{\alpha\Delta T}{(1-2\nu)}\begin{bmatrix}1\\1\\1\\0\\0\\0\end{bmatrix}$$

Appendix 4

FEMLAB Model Code

A sample code to generate a model of thermoelastic damping in a beam with two fixed ends is shown below. This code generates the geometry, supplies the boundary conditions, specifies the mesh density, and finds the eigenmode of interest. It outputs the real and imaginary parts of the eigenvalue, and displays a figure of the flexural mode and temperature profile on a slice through the beam. (This code was generated automatically FEMLAB. The user interface was used to set up the model, which was then saved as this '.m' file.)

```
% FEMLAB Model M-file
% Generated 15-Apr-2002 12:33:46 by FEMLAB 2.2.0.183.

flclear fem
% FEMLAB Version
clear vrsn;
vrsn.name='FEMLAB 2.2';
vrsn.major=0;
vrsn.build=183;
fem.version=vrsn;

% Recorded command sequence

% New geometry 1
fem.sdim={'x','y','z'};

% Geometry
tmp=rect2(0,250,0,50,0);
g1=extrude(tmp,'Distance',30,'Scale',[1;1],'Displ',[0;0],'Wrkpln',[0 1 0;0 ...
0 1;0 0 0]);

clear s f c p
objs={g1};
```

```
name={'EXT1'};
s.objs=objs;
s.name=name;

objs={};
name={};
f.objs=objs;
f.name=name;

objs={};
name={};
c.objs=objs;
c.name=name;

objs={};
name={};
p.objs=objs;
p.name=name;

drawstruct=struct('s',s,'f',f,'c',c,'p',p);
fem.draw=drawstruct;
fem.geom=geomcsg(fem);

clear appl

% Application mode 1
appl{1}.mode=flpdec3d(7,'dim',{'u','u_t','v','v_t','w','w_t','T','u_t', ...
'u_t_t','v_t','v_t_t','w_t','w_t_t','T_t'},'sdim',{'x','y','z'},'submode', ...
'std','tdiff','on');
appl{1}.dim={'u','u_t','v','v_t','w','w_t','T','u_t','u_t_t','v_t','v_t_t', ...
'w_t','w_t_t','T_t'};
appl{1}.form='coefficient';
appl{1}.border='off';
appl{1}.name='3D TED';
appl{1}.var={};
appl{1}.assign={'abscu1x';'abscu1x';'abscu2x';'abscu2x';'abscu3x';'abscu3x'; ...
'abscu4x';'abscu4x';'abscu5x';'abscu5x';'abscu6x';'abscu6x';'abscu7x'; ...
```

```
'abscu7x';'absga1x';'absga1x';'absga2x';'absga2x';'absga3x';'absga3x'; ...
'absga4x';'absga4x';'absga5x';'absga5x';'absga6x';'absga6x';'absga7x'; ...
'absga7x';'absu1x';'absux';'absu2x';'absu_tx';'absu3x';'absvx';'absu4x'; ...
'absv_tx';'absu5x';'abswx';'absu6x';'absw_tx';'absu7x';'absTx'};
appl{1}.elemdefault='Lag2';
appl{1}.shape={'shlag(2,''u'')','shlag(2,''u_t'')','shlag(2,''v'')', ...
'shlag(2,''v_t'')','shlag(2,''w'')','shlag(2,''w_t'')','shlag(2,''T'')'};
appl{1}.sshape=2;
appl{1}.equ.da={{{'1'},{'0'},{'0'},{'0'},{'0'},{'0'},{'0'};{'0'},{'1'}, ...
{'0'},{'0'},{'0'},{'0'},{'0'};{'0'},{'0'},{'1'},{'0'},{'0'},{'0'},{'0'}; ...
{'0'},{'0'},{'0'},{'1'},{'0'},{'0'},{'0'};{'0'},{'0'},{'0'},{'0'},{'1'}, ...
{'0'},{'0'};{'0'},{'0'},{'0'},{'0'},{'0'},{'1'},{'0'};{'0'},{'0'},{'0'}, ...
{'0'},{'0'},{'0'},{'1'}}};
appl{1}.equ.c={{{'1'},{'0'},{'0'},{'0'},{'0'},{'0'},{'0'};{'0'},{'1'},{'0'}, ...
{'0'},{'0'},{'0'},{'0'};{'0'},{'0'},{'1'},{'0'},{'0'},{'0'},{'0'};{'0'}, ...
{'0'},{'0'},{'1'},{'0'},{'0'},{'0'};{'0'},{'0'},{'0'},{'0'},{'1'},{'0'}, ...
{'0'};{'0'},{'0'},{'0'},{'0'},{'0'},{'1'},{'0'};{'0'},{'0'},{'0'},{'0'}, ...
{'0'},{'0'},{'1'}}};
appl{1}.equ.al={{{'0';'0';'0'},{'0';'0';'0'},{'0';'0';'0'},{'0';'0';'0'}, ...
{'0';'0';'0'},{'0';'0';'0'},{'0';'0';'0'};{'0';'0';'0'},{'0';'0';'0'},{'0'; ...
'0';'0'},{'0';'0';'0'},{'0';'0';'0'},{'0';'0';'0'},{'0';'0';'0'};{'0';'0'; ...
'0'},{'0';'0';'0'},{'0';'0';'0'},{'0';'0';'0'},{'0';'0';'0'},{'0';'0';'0'}, ...
{'0';'0';'0'};{'0';'0';'0'},{'0';'0';'0'},{'0';'0';'0'},{'0';'0';'0'},{'0'; ...
'0';'0'},{'0';'0';'0'},{'0';'0';'0'};{'0';'0';'0'},{'0';'0';'0'},{'0';'0'; ...
'0'},{'0';'0';'0'},{'0';'0';'0'},{'0';'0';'0'},{'0';'0';'0'};{'0';'0';'0'}, ...
{'0';'0';'0'},{'0';'0';'0'},{'0';'0';'0'},{'0';'0';'0'},{'0';'0';'0'},{'0'; ...
'0';'0'};{'0';'0';'0'},{'0';'0';'0'},{'0';'0';'0'},{'0';'0';'0'},{'0';'0'; ...
'0'},{'0';'0';'0'},{'0';'0';'0'}}};
appl{1}.equ.ga={{{'0';'0';'0'};{'0';'0';'0'};{'0';'0';'0'};{'0';'0';'0'}; ...
{'0';'0';'0'};{'0';'0';'0'};{'0';'0';'0'}}};
appl{1}.equ.be={{{'0';'0';'0'},{'0';'0';'0'},{'0';'0';'0'},{'0';'0';'0'}, ...
{'0';'0';'0'},{'0';'0';'0'},{'0';'0';'0'};{'0';'0';'0'},{'0';'0';'0'},{'0'; ...
'0';'0'},{'0';'0';'0'},{'0';'0';'0'},{'0';'0';'0'},{'0';'0';'0'};{'0';'0'; ...
'0'},{'0';'0';'0'},{'0';'0';'0'},{'0';'0';'0'},{'0';'0';'0'},{'0';'0';'0'}, ...
{'0';'0';'0'};{'0';'0';'0'},{'0';'0';'0'},{'0';'0';'0'},{'0';'0';'0'},{'0'; ...
'0';'0'},{'0';'0';'0'},{'0';'0';'0'};{'0';'0';'0'},{'0';'0';'0'},{'0';'0'; ...
'0'},{'0';'0';'0'},{'0';'0';'0'},{'0';'0';'0'},{'0';'0';'0'};{'0';'0';'0'}, ...
```

```
{'0';'0';'0'},{'0';'0';'0'},{'0';'0';'0'},{'0';'0';'0'},{'0';'0';'0'},{'0'; ...
'0';'0'};{'0';'0';'0'},{'0';'0';'0'},{'0';'0';'0'},{'0';'0';'0'},{'0';'0'; ...
'0'},{'0';'0';'0'},{'0';'0';'0'}}};
appl{1}.equ.a={{{'0'},{'0'},{'0'},{'0'},{'0'},{'0'},{'0'};{'0'},{'0'},{'0'}, ...
{'0'},{'0'},{'0'},{'0'};{'0'},{'0'},{'0'},{'0'},{'0'},{'0'},{'0'};{'0'}, ...
{'0'},{'0'},{'0'},{'0'},{'0'},{'0'};{'0'},{'0'},{'0'},{'0'},{'0'},{'0'}, ...
{'0'};{'0'},{'0'},{'0'},{'0'},{'0'},{'0'},{'0'},{'0'};{'0'},{'0'},{'0'},{'0'}, ...
{'0'},{'0'},{'0'}}};
appl{1}.equ.f={{{'1'};{'1'};{'1'};{'1'};{'1'};{'1'};{'1'}}};
appl{1}.equ.weak={{{'0'};{'0'};{'0'};{'0'};{'0'};{'0'};{'0'}}};
appl{1}.equ.dweak={{{'0'};{'0'};{'0'};{'0'};{'0'};{'0'};{'0'}}};
appl{1}.equ.constr={{{'0'};{'0'};{'0'};{'0'};{'0'};{'0'};{'0'}}};
appl{1}.equ.gporder={{4;4;4;4;4;4;4}};
appl{1}.equ.cporder={{2;2;2;2;2;2;2}};
appl{1}.equ.shape={1:7};
appl{1}.equ.init={{{'0'};{'0'};{'0'};{'0'};{'0'};{'0'};{'0'}}};
appl{1}.equ.usage={1};
appl{1}.equ.ind=1;
appl{1}.bnd.q={{{'0'},{'0'},{'0'},{'0'},{'0'},{'0'},{'0'};{'0'},{'0'},{'0'}, ...
{'0'},{'0'},{'0'},{'0'};{'0'},{'0'},{'0'},{'0'},{'0'},{'0'},{'0'};{'0'}, ...
{'0'},{'0'},{'0'},{'0'},{'0'},{'0'};{'0'},{'0'},{'0'},{'0'},{'0'},{'0'}, ...
{'0'};{'0'},{'0'},{'0'},{'0'},{'0'},{'0'},{'0'};{'0'},{'0'},{'0'},{'0'}, ...
{'0'},{'0'},{'0'}}};
appl{1}.bnd.g={{{'0'};{'0'};{'0'};{'0'};{'0'};{'0'};{'0'}}};
appl{1}.bnd.h={{{'1'},{'0'},{'0'},{'0'},{'0'},{'0'},{'0'};{'0'},{'1'},{'0'}, ...
{'0'},{'0'},{'0'},{'0'};{'0'},{'0'},{'1'},{'0'},{'0'},{'0'},{'0'};{'0'}, ...
{'0'},{'0'},{'1'},{'0'},{'0'},{'0'};{'0'},{'0'},{'0'},{'0'},{'1'},{'0'}, ...
{'0'};{'0'},{'0'},{'0'},{'0'},{'0'},{'1'},{'0'};{'0'},{'0'},{'0'},{'0'}, ...
{'0'},{'0'},{'1'}}};
appl{1}.bnd.r={{{'0'};{'0'};{'0'};{'0'};{'0'};{'0'};{'0'}}};
appl{1}.bnd.type={'dir'};
appl{1}.bnd.weak={{{'0'};{'0'};{'0'};{'0'};{'0'};{'0'};{'0'}}};
appl{1}.bnd.dweak={{{'0'};{'0'};{'0'};{'0'};{'0'};{'0'};{'0'}}};
appl{1}.bnd.constr={{{'0'};{'0'};{'0'};{'0'};{'0'};{'0'};{'0'}}};
appl{1}.bnd.gporder={{0;0;0;0;0;0;0}};
appl{1}.bnd.cporder={{0;0;0;0;0;0;0}};
appl{1}.bnd.shape={0};
```

```
appl{1}.bnd.ind=ones(1,6);
appl{1}.edg.weak={{{'0'};{'0'};{'0'};{'0'};{'0'};{'0'};{'0'}}};
appl{1}.edg.dweak={{{'0'};{'0'};{'0'};{'0'};{'0'};{'0'};{'0'}}};
appl{1}.edg.constr={{{'0'};{'0'};{'0'};{'0'};{'0'};{'0'};{'0'}}};
appl{1}.edg.gporder={{0;0;0;0;0;0;0}};
appl{1}.edg.cporder={{0;0;0;0;0;0;0}};
appl{1}.edg.shape={0};
appl{1}.edg.ind=ones(1,12);
appl{1}.pnt.weak={{{'0'};{'0'};{'0'};{'0'};{'0'};{'0'};{'0'}}};
appl{1}.pnt.dweak={{{'0'};{'0'};{'0'};{'0'};{'0'};{'0'};{'0'}}};
appl{1}.pnt.constr={{{'0'};{'0'};{'0'};{'0'};{'0'};{'0'};{'0'}}};
appl{1}.pnt.shape={0};
appl{1}.pnt.ind=ones(1,8);

fem.appl=appl;

% Initialize mesh
fem.mesh=meshinit(fem,...
        'Out',  {'mesh'},...
        'jiggle', 'on',...
        'Hcurve', 0.40000000000000002,...
        'Hcutoff',0.01,...
        'Hgrad', 1.3999999999999999,...
        'Hmaxfact',0.69999999999999996,...
        'Hmax',  {[],zeros(1,0),zeros(1,0),zeros(1,0),zeros(1,0)});

% Problem form
fem.outform='coefficient';

% Differentiation
fem.diff={'expr'};

% Differentiation simplification
fem.simplify='on';

% Point settings
clear pnt
```

```
pnt.weak={{{'0'};{'0'};{'0'};{'0'};{'0'};{'0'};{'0'}}};
pnt.dweak={{{'0'};{'0'};{'0'};{'0'};{'0'};{'0'};{'0'}}};
pnt.constr={{{'0'};{'0'};{'0'};{'0'};{'0'};{'0'};{'0'}}};
pnt.shape={0};
pnt.ind=ones(1,8);
fem.appl{1}.pnt=pnt;

% Edge settings
clear edg
edg.weak={{{'0'};{'0'};{'0'};{'0'};{'0'};{'0'};{'0'}}};
edg.dweak={{{'0'};{'0'};{'0'};{'0'};{'0'};{'0'};{'0'}}};
edg.constr={{{'0'};{'0'};{'0'};{'0'};{'0'};{'0'};{'0'}}};
edg.gporder={{0;0;0;0;0;0;0}};
edg.cporder={{0;0;0;0;0;0;0}};
edg.shape={0};
edg.ind=ones(1,12);
fem.appl{1}.edg=edg;

% Boundary conditions
clear bnd
bnd.q={{{'0'},{'0'},{'0'},{'0'},{'0'},{'0'},{'0'};{'0'},{'0'},{'0 },{'0'}, ...
{'0'},{'0'},{'0'};{'0'},{'0'},{'0'},{'0'},{'0'},{'0'},{'0'};{'0'},{'0'}, ...
{'0'},{'0'},{'0'},{'0'},{'0'};{'0'},{'0'},{'0'},{'0'},{'0'},{'0'},{'0'}; ...
{'0'},{'0'},{'0'},{'0'},{'0'},{'0'},{'0'};{'0'},{'0'},{'0'},{'0'},{'0'}, ...
{'0'},{'0'}},{{'0'},{'0'},{'0'},{'0'},{'0'},{'0'},{'0'};{'0'},{'0'},{'0'}, ...
{'0'},{'0'},{'0'},{'0'};{'0'},{'0'},{'0'},{'0'},{'0'},{'0'};{'0'}, ...
{'0'},{'0'},{'0'},{'0'},{'0'},{'0'};{'0'},{'0'},{'0'},{'0'},{'0'}, ...
{'0'};{'0'},{'0'},{'0'},{'0'},{'0'},{'0'},{'0'};{'0'},{'0'},{'0'},{'0'}, ...
{'0'},{'0'},{'0'}},{{'0'},{'0'},{'0'},{'0'},{'0'},{'0'},{'0'};{'0'},{'0'}, ...
{'0'},{'0'},{'0'},{'0'},{'0'};{'0'},{'0'},{'0'},{'0'},{'0'},{'0'},{'0'}; ...
{'0'},{'0'},{'0'},{'0'},{'0'},{'0'},{'0'};{'0'},{'0'},{'0'},{'0'},{'0'}, ...
{'0'},{'0'};{'0'},{'0'},{'0'},{'0'},{'0'},{'0'},{'0'};{'0'},{'0'},{'0'}, ...
{'0'},{'0'},{'0'},{'0'}}};
bnd.g={{{'0'};{'0'};{'0'};{'0'};{'0'};{'0'};{'0'}},{{'0'};{'0'};{'0'};{'0'}; ...
{'0'};{'0'};{'0'}},{{'0'};{'0'};{'0'};{'0'};{'0'};{'0'};{'0'}}};
bnd.h={{{'1'},{'0'},{'0'},{'0'},{'0'},{'0'},{'0'};{'0'},{'1'},{'0'},{'0'}, ...
{'0'},{'0'},{'0'};{'0'},{'0'},{'1'},{'0'},{'0'},{'0'},{'0'};{'0'},{'0'}, ...
```

```
{'0'},{'1'},{'0'},{'0'},{'0'};{'0'},{'0'},{'0'},{'0'},{'1'},{'0'},{'0'}; ...
{'0'},{'0'},{'0'},{'0'},{'0'},{'1'},{'0'};{'0'},{'0'},{'0'},{'0'},{'0'}, ...
{'0'},{'0'}},{{'0'},{'0'},{'0'},{'0'},{'0'},{'0'},{'0'};{'0'},{'0'},{'0'}, ...
{'0'},{'0'},{'0'},{'0'};{'0'},{'0'},{'0'},{'0'},{'0'},{'0'},{'0'};{'0'}, ...
{'0'},{'0'},{'0'},{'0'},{'0'},{'0'};{'0'},{'0'},{'0'},{'0'},{'0'},{'0'}, ...
{'0'};{'0'},{'0'},{'0'},{'0'},{'0'},{'0'},{'0'};{'0'},{'0'},{'0'},{'0'}, ...
{'0'},{'0'},{'0'}},{{'1'},{'0'},{'0'},{'0'},{'0'},{'0'},{'0'};{'0'},{'1'}, ...
{'0'},{'0'},{'0'},{'0'},{'0'};{'0'},{'0'},{'0'},{'0'},{'0'},{'0'},{'0'}; ...
{'0'},{'0'},{'0'},{'0'},{'0'},{'0'},{'0'};{'0'},{'0'},{'0'},{'0'},{'0'}, ...
{'0'},{'0'};{'0'},{'0'},{'0'},{'0'},{'0'},{'0'},{'0'};{'0'},{'0'},{'0'}, ...
{'0'},{'0'},{'0'},{'0'}}};
bnd.r={{{'0'};{'0'};{'0'};{'0'};{'0'};{'0'};{'0'}},{{'0'};{'0'};{'0'};{'0'}; ...
{'0'};{'0'};{'0'}},{{'0'};{'0'};{'0'};{'0'};{'0'};{'0'};{'0'}}};
bnd.type={'dir','dir','dir'};
bnd.weak={{{'0'};{'0'};{'0'};{'0'};{'0'};{'0'};{'0'}},{{'0'};{'0'};{'0'}; ...
{'0'};{'0'};{'0'};{'0'}},{{'0'};{'0'};{'0'};{'0'};{'0'};{'0'};{'0'}}};
bnd.dweak={{{'0'};{'0'};{'0'};{'0'};{'0'};{'0'};{'0'}},{{'0'};{'0'};{'0'}; ...
{'0'};{'0'};{'0'};{'0'}},{{'0'};{'0'};{'0'};{'0'};{'0'};{'0'};{'0'}}};
bnd.constr={{{'0'};{'0'};{'0'};{'0'};{'0'};{'0'};{'0'}},{{'0'};{'0'};{'0'}; ...
{'0'};{'0'};{'0'};{'0'}},{{'0'};{'0'};{'0'};{'0'};{'0'};{'0'};{'0'}}};
bnd.gporder={{0;0;0;0;0;0;0},{0;0;0;0;0;0;0},{0;0;0;0;0;0;0}};
bnd.cporder={{0;0;0;0;0;0;0},{0;0;0;0;0;0;0},{0;0;0;0;0;0;0}};
bnd.shape={0,0,0};
bnd.ind=[1 2 2 2 2 3];
fem.appl{1}.bnd=bnd;

% PDE coefficients
clear equ
equ.da={{{'i'},{'0'},{'0'},{'0'},{'0'},{'0'},{'0'};{'0'},{'-i'},{'0'},{'0'}, ...
{'0'},{'0'},{'0'};{'0'},{'0'},{'i'},{'0'},{'0'},{'0'},{'0'};{'0'},{'0'}, ...
{'0'},{'-i'},{'0'},{'0'},{'0'};{'0'},{'0'},{'0'},{'0'},{'i'},{'0'},{'0'}; ...
{'0'},{'0'},{'0'},{'0'},{'0'},{'-i'},{'0'};{'0'},{'0'},{'0'},{'0'},{'0'}, ...
{'0'},{'-i'}}};
equ.c={{{'0'},{'0'},{'0'},{'0'},{'0'},{'0'},{'0'};{'3.273';'1';'1'},{'0'}, ...
{'0','1.273','0';'1','0','0';'0','0','0'},{'0'},{'0','0','1.273';'0','0', ...
'0';'1','0','0'},{'0'},{'0'};{'0'},{'0'},{'0'},{'0'},{'0'},{'0'},{'0'};{'0', ...
'1','0';'1.273','0','0';'0','0','0'},{'0'},{'1';'3.273';'1'},{'0'},{'0','0', ...
```

```
'0';'0','0','1.273';'0','1','0'},{'0'},{'0'};{'0'},{'0'},{'0'},{'0'},{'0'}, ...
{'0'},{'0'};{'0','0','1';'0','0','0';'1.273','0','0'},{'0'},{'0','0','0'; ...
'0','0','1';'0','1.273','0'},{'0'},{'1';'1';'3.273'},{'0'},{'0'};{'0'}, ...
{'0'},{'0'},{'0'},{'0'},{'0'},{'1'}}};
equ.al={{{'0';'0';'0'},{'0';'0';'0'},{'0';'0';'0'},{'0';'0';'0'},{'0';'0'; ...
'0'},{'0';'0';'0'},{'0';'0';'0'};{'0';'0';'0'},{'0';'0';'0'},{'0';'0';'0'}, ...
{'0';'0';'0'},{'0';'0';'0'},{'0';'0';'0'},{'-coup';'0';'0'};{'0';'0';'0'}, ...
{'0';'0';'0'},{'0';'0';'0'},{'0';'0';'0'},{'0';'0';'0'},{'0';'0';'0'},{'0'; ...
'0';'0'};{'0';'0';'0'},{'0';'0';'0'},{'0';'0';'0'},{'0';'0';'0'},{'0';'0'; ...
'0'},{'0';'0';'0'},{'0';'-coup';'0'};{'0';'0';'0'},{'0';'0';'0'},{'0';'0'; ...
'0'},{'0';'0';'0'},{'0';'0';'0'},{'0';'0';'0'},{'0';'0';'0'};{'0';'0';'0'}, ...
{'0';'0';'0'},{'0';'0';'0'},{'0';'0';'0'},{'0';'0';'0'},{'0';'0';'0'},{'0'; ...
'0';'-coup'};{'0';'0';'0'},{'0';'0';'0'},{'0';'0';'0'},{'0';'0';'0'},{'0'; ...
'0';'0'},{'0';'0';'0'},{'0';'0';'0'}}};
equ.ga={{{'0';'0';'0'};{'0';'0';'0'};{'0';'0';'0'};{'0';'0';'0'};{'0';'0'; ...
'0'};{'0';'0';'0'};{'0';'0';'0'}}};
equ.be={{{'0';'0';'0'},{'0';'0';'0'},{'0';'0';'0'},{'0';'0';'0'},{'0';'0'; ...
'0'},{'0';'0';'0'},{'0';'0';'0'};{'0';'0';'0'},{'0';'0';'0'},{'0';'0';'0'}, ...
{'0';'0';'0'},{'0';'0';'0'},{'0';'0';'0'},{'0';'0';'0'};{'0';'0';'0'},{'0'; ...
'0';'0'},{'0';'0';'0'},{'0';'0';'0'},{'0';'0';'0'},{'0';'0';'0'},{'0';'0'; ...
'0'};{'0';'0';'0'},{'0';'0';'0'},{'0';'0';'0'},{'0';'0';'0'},{'0';'0';'0'}, ...
{'0';'0';'0'},{'0';'0';'0'};{'0';'0';'0'},{'0';'0';'0'},{'0';'0';'0'},{'0'; ...
'0';'0'},{'0';'0';'0'},{'0';'0';'0'},{'0';'0';'0'};{'0';'0';'0'},{'0';'0'; ...
'0'},{'0';'0';'0'},{'0';'0';'0'},{'0';'0';'0'},{'0';'0';'0'},{'0';'0';'0'}; ...
{'0';'0';'0'},{'coup';'0';'0'},{'0';'0';'0'},{'0';'coup';'0'},{'0';'0';'0'}, ...
{'0';'0';'coup'},{'0';'0';'0'}}};
equ.a={{{'0'},{'1'},{'0'},{'0'},{'0'},{'0'},{'0'};{'0'},{'0'},{'0'},{'0'}, ...
{'0'},{'0'},{'0'};{'0'},{'0'},{'0'},{'1'},{'0'},{'0'},{'0'};{'0'},{'0'}, ...
{'0'},{'0'},{'0'},{'0'},{'0'};{'0'},{'0'},{'0'},{'0'},{'0'},{'1'},{'0'}; ...
{'0'},{'0'},{'0'},{'0'},{'0'},{'0'},{'0'};{'0'},{'0'},{'0'},{'0'},{'0'}, ...
{'0'},{'0'}}};
equ.f={{{'0'};{'0'};{'0'};{'0'};{'0'};{'0'};{'0'}}};
equ.weak={{{'0'};{'0'};{'0'};{'0'};{'0'};{'0'};{'0'}}};
equ.dweak={{{'0'};{'0'};{'0'};{'0'};{'0'};{'0'};{'0'}}};
equ.constr={{{'0'};{'0'};{'0'};{'0'};{'0'};{'0'};{'0'}}};
equ.gporder={{4;4;4;4;4;4;4}};
equ.cporder={{2;2;2;2;2;2;2}};
```

```
equ.shape={1:7};
equ.init={{{'0'};{'0'};{'0'};{'0'};{'0'};{'0'};{'0'}}};
equ.usage={1};
equ.ind=1;
fem.appl{1}.equ=equ;

% Internal borders
fem.appl{1}.border='off';

% Shape functions
fem.appl{1}.shape={'shlag(2,''u'')','shlag(2,''u_t'')','shlag(2,''v'')','shlag(2,''v_t'')','shlag(2,''w'')','shla
g(2,''w_t'')','shlag(2,''T'')'};

% Geometry element order
fem.appl{1}.sshape=2;

% Differentiation rules
fem.rules={};

% Define variables
fem.variables={'coup', 0.046199999999999998};

% Multiphysics
fem=multiphysics(fem);

% Extend the mesh
fem.xmesh=meshextend(fem,'context','local','cplbndeq','on','cplbndsh','on');

% Evaluate initial condition
init=asseminit(fem,...
        'context','local',...
        'init',  fem.xmesh.eleminit);

% Solve eigenvalue problem
fem.sol=femeig(fem,...
        'eigfun', 'fleig',...
        'eigpar', {1,0.00197},...
```

```
        'stop',  'on',...
        'u',     init.u,...
        'jacobian','equ',...
        'report', 'on',...
        'context','local',...
        'sd',    'off',...
        'nullfun','flnullorth',...
        'blocksize',5000,...
        'solcomp',{'T','u','u_t','v','v_t','w','w_t'},...
        'linsolver','matlab',...
        'method', 'eliminate',...
        'out',   'sol');

% Save current fem structure for restart purposes
fem0=fem;

% Plot solution
postplot(fem,...
        'geomnum',1,...
        'context','local',...
        'tetdata',{'T','cont','internal'},...
        'tetfacestyle','interp',...
        'tetedgestyle','none',...
        'tetkeep',1,...
        'tetkeeptype','random',...
        'tetmap', 'jet',...
        'tetmaxmin','off',...
        'tetbar', 'on',...
        'deformdata',{{'u','cont','internal'},{'v','cont','internal'},{'w','cont','internal'}},...
        'deformmaxmin','off',...
        'deformauto','on',...
        'geom',  'on',...
        'geomcol','bginv',...
        'refine', 3,...
        'contorder',2,...
        'phase',  0,...
        'lightmodel','phong',...
```

```
'lightreflection','default',...
'transparency',1,...
'view',  [-37.500000000000007 29.999999999999986],...
'title', 'Lambda(1)=0.00195435+6.01107e-008i  Tetrahedron: T (T)  Displacement: [u (u),v
(v),w (w)]  ',...
'solnum', 1,...
'renderer','zbuffer',...
'scenelight','off',...
'camlight','off',...
'campos', [-736.07791986613643 -1054.5979588418452 807.93757635768509],...
'camprojection','orthographic',...
'camtarget',[100 35 15],...
'camup',  [0 0 1],...
'camva',  20.921046564263793,...
'axispos',[-0.25750000000000001 -0.29749999999999999 1.55 1.6299999999999999],...
'axisequal','on',...
'axis',  [-50 250 -10 80 -10 40],...
'axisvisible','on',...
'grid',  'on',...
'scenelightpos',[-736.07791986613643 -1054.5979588418452 807.93757635768509])
```

References

[1] Zener, Clarence, "Internal Friction in Solids, I. Theory of Internal Friction in Reeds", *Physical Review*, Vol. 52, Aug. 1, 1937, pp. 230-235.

[2] Zener, Clarence, "Internal Friction in Solids, II. General Theory of Thermoelastic Internal Friction", *Physical Review*, Vol. 53, Jan. 1, 1938, pp. 90-99.

[3] Lifshitz, Ron, and Roukes, M.L., "thermoelastic Damping in Micro- and Nanomechanical Systems", *Physical Review B*, Vol. 61, No. 8, pp. 5600-5609.

[4] Strunin, D. V., Melnik, R. V. N., Roberts, A. J., "Numerical modeling of thermoelastic processes using non-linear theories with thermal relaxation time", *The ANZIAM Journal*, Vol. 42, Nov. 2000, pp. 1356-1378.

[5] Givoli, Dan, Rand, Omri, "Harmonic finite-element thermoelastic analysis of space frames and trusses", *Journal of Thermal Stresses*, Vol. 16, No. 3, pp 233-248.

[6] Yasumura, Kevin Y., Stowe, Timothy D., Chow, Eugene M., Pfafman, Timothy, Kenney, Thomas W., Stipe, Barry C., and Rugar, Daniel, "Quality Factors in Micron- and Submicron- Thick Cantilevers", *Journal of Microelectromechanical Systems*, Vol. 9, No. 1, March 2000, pp. 117-125.

[7] C. Cabuz, C., Fukatsu, K., Kurabayashi, T., Minami, K., Esashi, M., "Microphysical Investigations on Mechanical Structures Realized in p+ Silicon", *Journal of Microelectromechanical Systems*, Vol. 4, No 3, pp. 109-118.

[8] Okada, Y., "Diamond Cubic Si: structure, lattice parameter and density," *The Properties of Crystalline Silicon*, ed. Robert Hull, INSPEC, The Institution of Electrical Engineers, London, 1999.

[9] http://www.webelements.com

[10] Kagaya, H.-M., Soma, T., "Specific Heats of c-Si and molten Si," *The Properties of Crystalline Silicon*, ed. Robert Hull, INSPEC, The Institution of Electrical Engineers, London, 1999.

[11] J. Dismukes, L. Ekstrom, E. Steigmeier, I. Kudman, D. Beers, "Thermal and Electrical Properties of Heavily Doped Ge-Si Alloys up to 1300K", *Journal of Applied Physics*, Vol. 35, No. 10, pp. 2899-2907.

[12] K.L. Wang, X. Zheng, "Thermal properties of SiGe," *Properties of Strained and Relaxed Silicon Germanium*, ed. Erich Kasper, INSPEC, The Institution of Electrical Engineers, London, 1995.

[13] Kittel, Charles, "Phonons II. Thermal Properties", *Introduction to Solid State Physics*, 7th ed., John Wiley & Sons, Inc., New York, 1996, pp.137-138.

[14] Properties of Silicon, EMIS Datareviews Series No. 4, INSPEC, The Institution of Electrical Engineers, London, 1988.

Bibliography

Braginsky, V.B., Mitrofanov, V.P., and Panov, V.I., *Systems with Small Dissipation*, The University of Chicago Press, Chicago, 1986.

Fowles, Grant R., "The Harmonic Oscillator", *Analytical Mechanics*, 4th ed, Saunders College Publishing, New York, 1986, pp. 55-83.

Hsu, Tai-Ran, *The Finite Element Method in Thermomechanics*, Allen & Unwin, Boston, 1986.

Moaveni, Saeed, *Finite Element Analysis- Theory and Application with Ansys*, Prentice Hall, New Jersey, 1999.

Nowacki, Witold, "Basic Relations and Equations of Thermoelasticity", *Thermoelasticity*, 2nd ed., Pergamon Press, New York, 1986.

Nowick, A.S., and Berry, B.S., *Anelastic Relaxation in Crystalline Solids*, Academic Press, New York, 1972.

Senturia, Stephen D., *Microsystem Design*, Kluwer Academic Publishers, 2001.

Zemansky, Mark W., Dittman, Richard H., *Heat and Thermodynamics*, 7th ed., McGraw-Hill, New York, 1997.

THESIS PROCESSING SLIP

FIXED FIELD: ill. _____ name _____

index _____ biblio _____

►**COPIES:** (Archives) Aero Dewey Barker Hum

Lindgren Music Rotch (Science) Sche-Plough

TITLE VARIES: ►☑ Finite Element Analysis

NAME VARIES: ►☑ Patrick

IMPRINT: **(COPYRIGHT)** _____

►**COLLATION:** _____

►**ADD: DEGREE:** _____ ►**DEPT.:** _____

►**ADD: DEGREE:** _____ ►**DEPT.:** _____

SUPERVISORS: _____

NOTES:

cat'r: date:

page: ▶ J 75

►**DEPT:** Mat Sci & E

►**YEAR:** 2002 ►**DEGREE:** S.M.

►**NAME:** GORMAN, John P.